Bulletin of the Seismological Society of America, Vol. 94, No. 6B, pp. S85–S106, December 2004

Ⓔ

Seismic Velocity Models for the Denali Fault Zone along the Richardson Highway, Alaska

by Thomas M. Brocher, Gary S. Fuis, William J. Lutter, Nikolas I. Christensen, and Natalia A. Ratchkovski

Abstract Crustal-scale seismic-velocity models across the Denali fault zone along the Richardson Highway show a 50-km-thick crust, a near vertical fault trace, and a 5-km-wide damage zone associated with the fault near Trans-Alaska Pipeline Pump Station 10, which provided the closest strong ground motion recordings of the 2002 Denali fault earthquake. We compare models, derived from seismic reflection and refraction surveys acquired in 1986 and 1987, to laboratory measurements of seismic velocities for typical metamorphic rocks exposed along the profiles. Our model for the 1986 seismic reflection profile indicates a 5-km-wide low-velocity zone in the upper 1 km of the Denali fault zone, which we interpret as fault gouge. Deeper refractions from our 1987 line image a 40-km wide, 5-km-deep low-velocity zone along the Denali fault and nearby associated fault strands, which we attribute to a composite damage zone along several strands of the Denali fault zone and to the obliquity of the seismic line to the fault zone. Our velocity model and other geophysical data indicate a nearly vertical Denali fault zone to a depth of 30 km. Aftershocks of the 2002 Denali fault earthquake and our velocity model provide evidence for a flower structure along the fault zone consisting of faults dipping toward and truncated by the Denali fault. Wide-angle reflections indicate that the crustal thickness beneath the Denali fault is transitional between the 60-km-thick crust beneath the Alaska Range to the south, and the extended, 30-km-thick crust of the Yukon–Tanana terrane to the north.

Online Material: Tables of locations for the TACT 1986 and TACT 1987 lines.

Introduction

The November 2002 M_w 7.9 Denali fault earthquake was the largest inland strike-slip event to strike North America since the 1906 San Francisco earthquake in California (Eberhart-Phillips *et al.*, 2003; Frankel, 2004). The earthquake yielded a number of valuable strong ground motion recordings, measurements of surface rupture, geodetic observations, and other instrumental recordings. Strong ground motions from the earthquake were recorded as near as 3 km from the surface rupture, at Trans-Alaska Pipeline Pump Station 10, where the largest peak accelerations of 0.36*g* were observed (Ellsworth *et al.*, 2004). Finite-source and geodetic inversions of fault slip reveal that the Richardson Highway was located within one of three large slip patches produced by the earthquake (Eberhart-Phillips *et al.*, 2003; Frankel, 2005). Coseismic slip reached 5.8 m (dextral slip) at the Richardson Highway (Haeussler *et al.*, 2005).

Stout *et al.* (1973) estimated the long-term right-lateral slip rate on the Denali fault near the Richardson Highway as 5 to 6 mm/yr based on offset Holocene alluvial fans and drainages. Plafker *et al.* (1977) estimated this rate as 10 mm/yr based on offsets of inferred Wisconsin-age moraines. Fletcher (2002) inverted Global Positioning System (GPS) measurements across the fault as indicating a slip rate of 8 mm/yr with an apparent geodetic locking depth of 28 km.

Along the Richardson Highway, the Denali fault zone takes a right-hand extensional bend (Fig. 1A). Relatively few aftershocks were recorded along the highway (Fig. 1B), although many aftershocks were recorded to the west and east of the extensional bend (Ratchkovski *et al.*, 2003). East of the Richardson Highway, the Denali fault splays into several associated faults, including the Broxson Gulch thrust and the Hines Creek fault (Fig. 1B). West of the highway, aftershocks of the Denali fault earthquake occupy a broad area centered on the Denali fault zone (Fig. 1B), suggesting that several of these associated faults experienced postseismic slip (Ratchkovski *et al.*, 2003).

Trans-Alaska Crustal Transect (TACT) Seismic Lines

In 1986, the U.S. Geological Survey (USGS) acquired an 83.9-km-long deep crustal seismic reflection line crossing

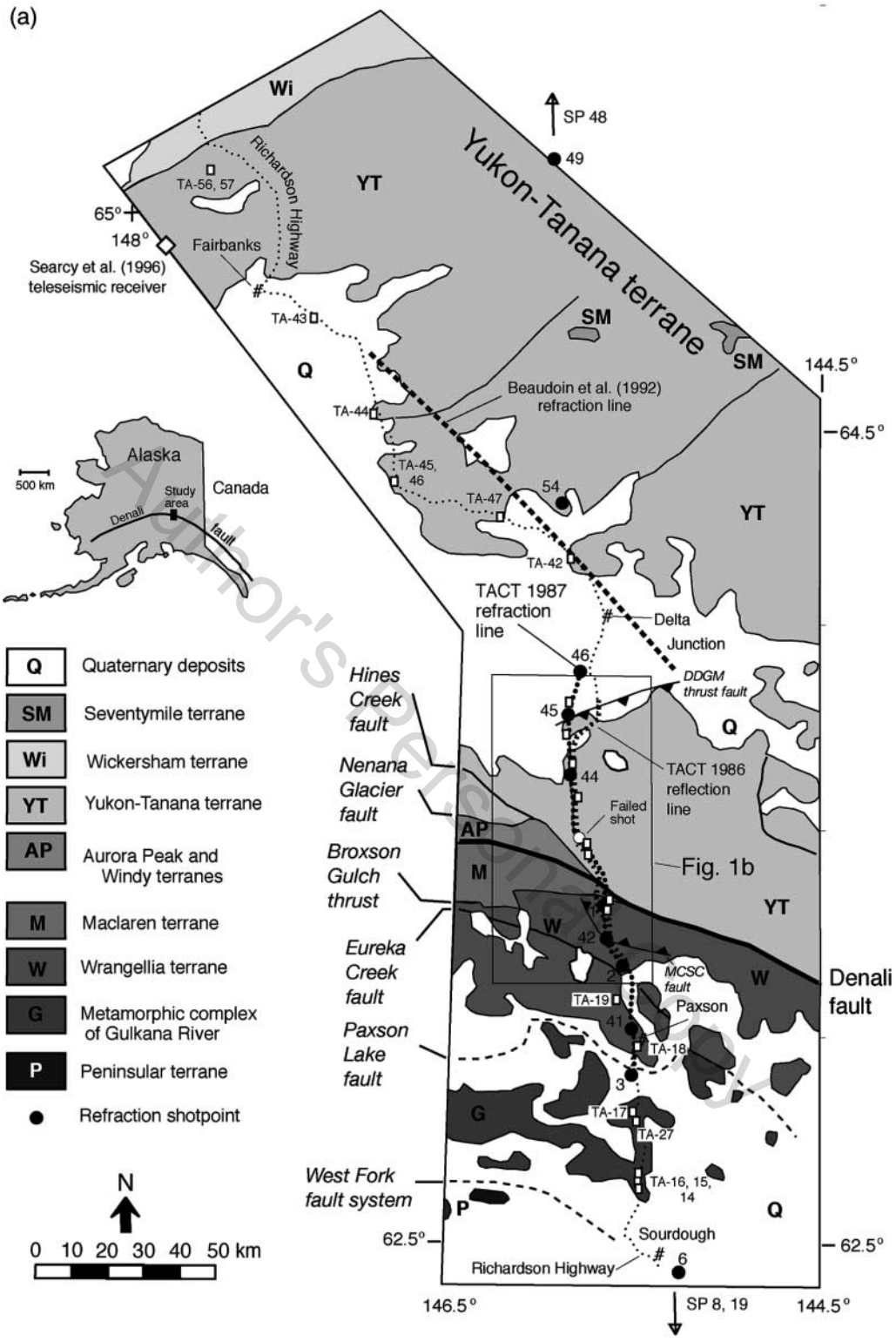

Figure 1. (A) Map showing location of seismic lines along the Richardson Highway crossing the Denali fault zone acquired by the Trans-Alaska Crustal Transect (TACT) project. Thick dotted line shows location of the TACT 1987 line. Thinner dashed line shows location of TACT 1986 line (Fisher *et al.*, 2004). Beaudoin *et al.*'s (1992) refraction line in Yukon–Tanana terrane is shown as a heavy dashed line. Base geological map is adapted from Foster *et al.* (1987), Jones *et al.* (1987), and Nokleberg *et al.* (1989). Faults are dashed where inferred. Figure modified from Brocher *et al.* (1991). (*continued*)

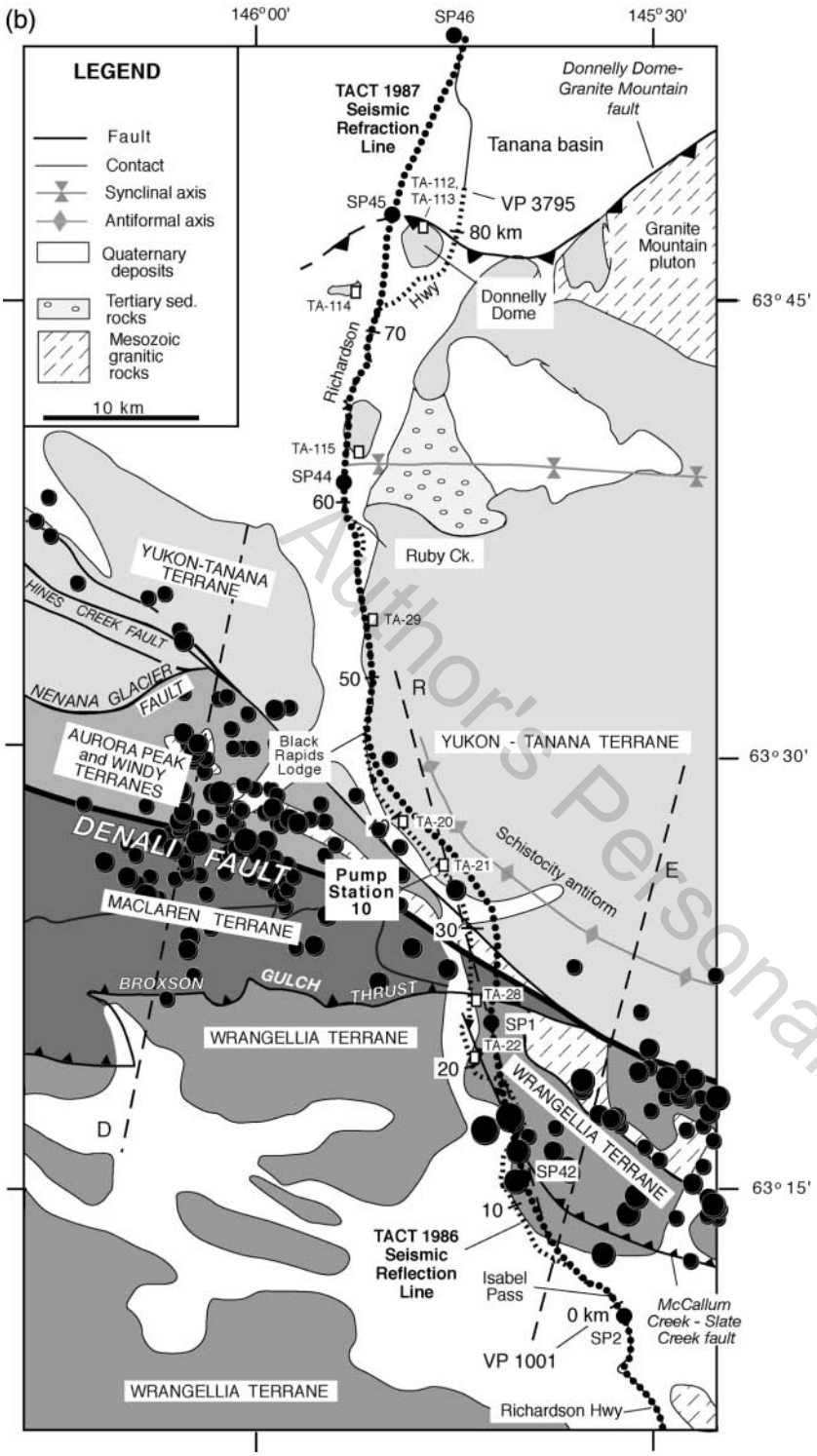

Figure 1. (*continued*) (B) Detail map of study area. Dashed lines labeled C, E, and R provide locations of cross sections showing relocated aftershocks of the 2002 Denali fault earthquake plotted in Figure 9 (Ratchkovski *et al.*, 2003). Numbers 0, 10, 20, 30, etc., along TACT 1986 line mark model kilometers along the line. Aftershock locations are from the Advanced National Seismic System (ANSS) online catalog. DDGM, Donnelly Dome–Granite Mountain; MCSC, McCallum Creek–Slate Creek.

the Alaska Range and the Denali fault zone along the Richardson Highway (Fisher *et al.*, 2004), which we will refer to as the TACT 1986 line. The line, collected for the TACT project (Stone *et al.*, 1986), ran along the Trans-Alaska Pipeline. The line started at the Richardson Monument and ended just north of Donnelly Dome (Fig. 1B).

The TACT 1986 line was acquired using a recording array providing source-receiver offsets up to 15 km. Brocher *et al.* (1991) used travel times recorded to these offsets to derive compressional- and shear-wave velocity models for the shallow upper crust along the Richardson Highway (Fig. 2). Although the line passes through Isabel Pass and the Alaska Range (Fig. 1B) there is only 460 m of vertical

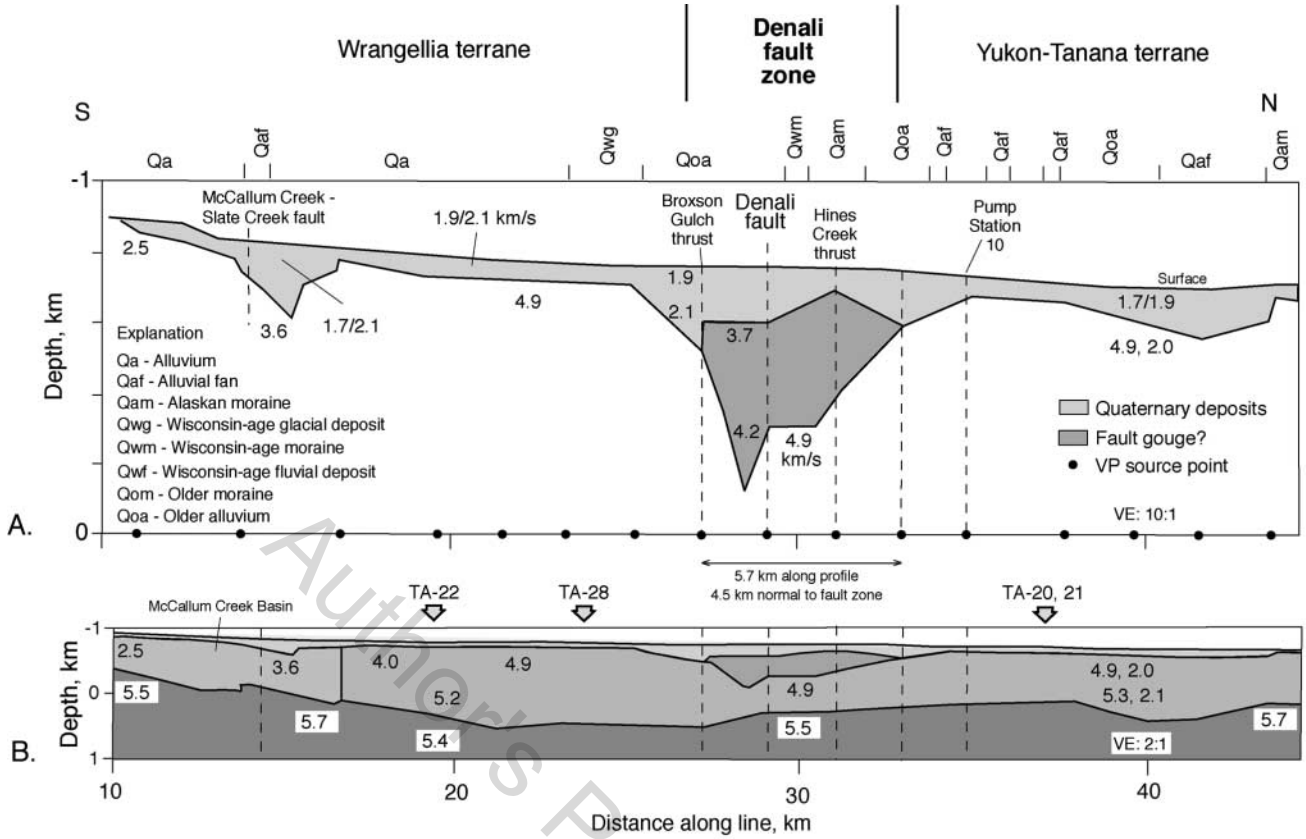

Figure 2. (A) Comparison of mapped Quaternary deposits along the TACT 1986 line with velocity model inferred from forward modeling of refracted arrivals for the line. Numbers along model indicate compressional-wave velocities in km/sec. A slash between two numbers indicates a vertical velocity gradient between the numbers given. Dots along the base of the model show the horizontal location of the sources used for forward modeling. Distances along the model correspond to km markers shown in Figure 1B. (B) Same velocity model for the TACT 1986 line showing velocities within the Devonian and upper Mesozoic metamorphic basement rocks. At km 40, shear-wave velocities are shown after the corresponding compressional-wave velocities, with a comma separating the two velocities. Locations of rocks sampled for laboratory measurements are indicated by large arrows with sample numbers (e.g., TA-22). Figure modified from Brocher *et al.* (1991).

relief along it. (Ⓔ Coordinates for this line are available online at the SSA Web site).

In 1987, the USGS acquired a 115-km-long seismic refraction line crossing the Denali fault along the Richardson Highway (Beaudoin *et al.*, 1989). Eight large borehole explosions were detonated within the line of recorders, and six explosions to the north and south of the line provided wide-angle coverage of the lower crust and Moho (Fig. 1A). Crustal models for this refraction line, which we call the TACT 1987 line, have not been reported.

In this study we integrate the results of the two TACT seismic lines, compare the results to laboratory studies of typical metamorphic rock suites found along the Richardson Highway and to the isostatic gravity field, and discuss some of the implications of the models for understanding the structure of the Denali fault and strong ground motions produced by the 2002 Denali fault earthquake.

Geologic Setting

The geology along the TACT seismic lines in the Alaska Range has been previously summarized (e.g., Nokleberg *et al.*, 1982, 1985, 1986, 1992a, 1992b; Jones *et al.*, 1987; Stanley *et al.*, 1990; Ridgway *et al.*, 1997, 2002). We focus on the Wrangellia and Yukon–Tanana terranes, which, by area, comprise the majority of the units exposed at the surface along the seismic lines (Fig. 1B). The Wrangellia terrane is interpreted as a late Paleozoic island arc overlain by Mesozoic basaltic and island arc volcanic rocks and flysch. Very few, if any, of these Mesozoic cover rocks are preserved in the study area. The Yukon–Tanana terrane consists of Devonian and older metasedimentary schists and sparse Devonian metavolcanic and metagranitic rocks (Aleinikoff and Nokleberg, 1985; Nokleberg and Aleinikoff, 1985; Foster *et al.*, 1987; Jones *et al.*, 1987). In addition, we consider

the Kahiltna Formation, largely Upper Jurassic and Lower Cretaceous flysch and associated andesitic volcanic rocks, which may have been underthrust along the Denali fault zone during the mid-Cretaceous (Jones *et al.*, 1987; Stanley *et al.*, 1990).

North of the Denali fault, in the Yukon–Tanana terrane, the schistocity is folded into a large antiform (Fig. 1A). Brocher *et al.* (1991) cited a large anisotropy in laboratory measurements of compressional wave velocities to support their inference that this schistocity antiform is responsible for a northward increase in compressional wave velocities north of the Denali fault.

The valley occupied by the Richardson Highway in this location is underlain by a thin, typically 50 to 100 m thick, veneer of Quaternary deposits and weathered bedrock (Brocher *et al.*, 1991). These Quaternary units are alluvial or moraine deposits of various ages (Fig. 2). They thicken slightly in the vicinity of the McCallum Creek-Slate Creek and Denali fault zones.

The TACT 1986 Seismic Reflection Line

Forward modeling of first-arrival travel times from the TACT 1986 line (Brocher *et al.*, 1991) indicates that the compressional-wave velocities of the uppermost deposits lie between 1.7 and 2.1 km/sec (Fig. 2A) which are typical of Quaternary glacial deposits. Shear-wave velocities for these deposits derived from forward modeling of the secondary arrivals from the TACT 1986 reflection line range between 0.6 and 1.6 km/sec (Brocher *et al.*, 1991).

Two distinct travel-time branches having different apparent velocities, and a pronounced seismic reflection (Brocher *et al.*, 1991), provide evidence that the contact between the Quaternary deposits and the metamorphic basement rocks is a strong velocity discontinuity. In our velocity model for this contact (Fig. 2), compressional-wave velocities in the metamorphic bedrock in both the Wrangellia and Yukon–Tanana terranes increase abruptly to 4.9 km/sec; the corresponding shear-wave velocity increases abruptly to 2.0 km/sec (Fig. 2).

Within the Wrangellia and Yukon–Tanana terrane basement rocks, where velocity gradients are lower and the tomography model is better resolved, comparison of the tomographic compressional- and shear-wave velocity models in the Yukon–Tanana terrane indicate that a V_p/V_s ratio of 2.0 is appropriate for the upper 1 km of these basement rocks (Fig. 3). Although we did not explicitly solve for V_p/V_s, and V_s is not as well resolved as V_p in this location, a higher V_p/V_s, 2.2–2.5, may be more appropriate for the vicinity of Pump Station 10.

In the Denali fault zone, the Quaternary deposits and top of the metamorphic basement rocks are separated by a 300- to 400-m-thick unit having a compressional-wave velocity of 3.7 to 4.2 km/sec (Fig. 2B). Although Brocher *et al.* (1991) interpreted this unit as Tertiary sedimentary strata, such Tertiary strata are not proximal to the fault. This observation, the unit's location along the Denali fault zone, and the strongly negative topographic expression of the fault zone suggest that a more plausible interpretation of this unit is that it represents fault-gouge or fault-damaged material. This zone of fault damage would be about 5.7 km wide along the TACT 1986 reflection line, which locally trended along the fault (Fig. 1B), but is closer to 4.5 km wide as measured normal to the Denali fault zone (Fig. 2A).

Description of the TACT 1987 Seismic Refraction Line

In 1987 the USGS, in cooperation with the Geological Survey of Canada, collected a 115-km-long seismic refraction/wide-angle reflection line across the Alaska Range between Paxson and Delta Junction (Fig. 1A). A total of 13 shots, varying in size between 455 and 2725 kg of ammonium nitrate, were recorded by 120 USGS cassette recorders having a nominal spacing of 1 km (Beaudoin *et al.*, 1989). (Ⓔ The source and receiver locations for the TACT 1987 line are available online at the SSA Web site).

Eight shots were detonated at intervals of about 15 km along the line in boreholes and lakes. Six shots detonated off the ends of the receiver lines produced maximum source-receiver offsets of 325 km (Fig. 1A). All shotholes were detonated either in rock or wet alluvium (Kohler and Fuis, 1992). Charges larger than 1360 kg were split evenly into two boreholes fired simultaneously. The 20-cm-diameter boreholes ranged in depth from 30 to 49 m (Brocher, 2003). The experimental uncertainties in timing were about one msec (Beaudoin *et al.*, 1989).

Compared to other TACT refraction lines, record sections from the TACT 1987 line show low signal-to-noise ratios (Fig. 4). These low ratios are attributed to several factors; weak coupling of the explosive energy into glacial till and stormy weather conditions were most important with higher background noise levels along the Trans-Alaska Pipeline and weak crustal reflectors likely being secondary factors. Shotpoints on the southern half of the line gave higher quality data than shotpoints on the northern end of the line (e.g., Fig. 4). The weak sources on the north end of the line (e.g., Shotpoints 45 and 46, detonated in glacial till) adversely affected our ability to correlate secondary, reflected arrivals on reversing profiles (Fig. 4). Nonetheless, these data constrain the velocity of the upper crust and the average velocity and thickness of the crust.

Compressional-wave refractions from the upper crust, *Pg*, having an apparent phase velocity of about 6 km/sec, are traceable to variable offsets (see examples in Fig. 4). Short, discontinuous wide-angle reflections from the middle and lower crust are observed in the record sections from shotpoints on both ends of the line. Short, wide-angle reflections from the top of the upper mantle, *PmP*, are observed only from the shots near the northern and southern ends of the line (Figs. 4, 5).

Refractions from the upper mantle, *Pn*, are observed

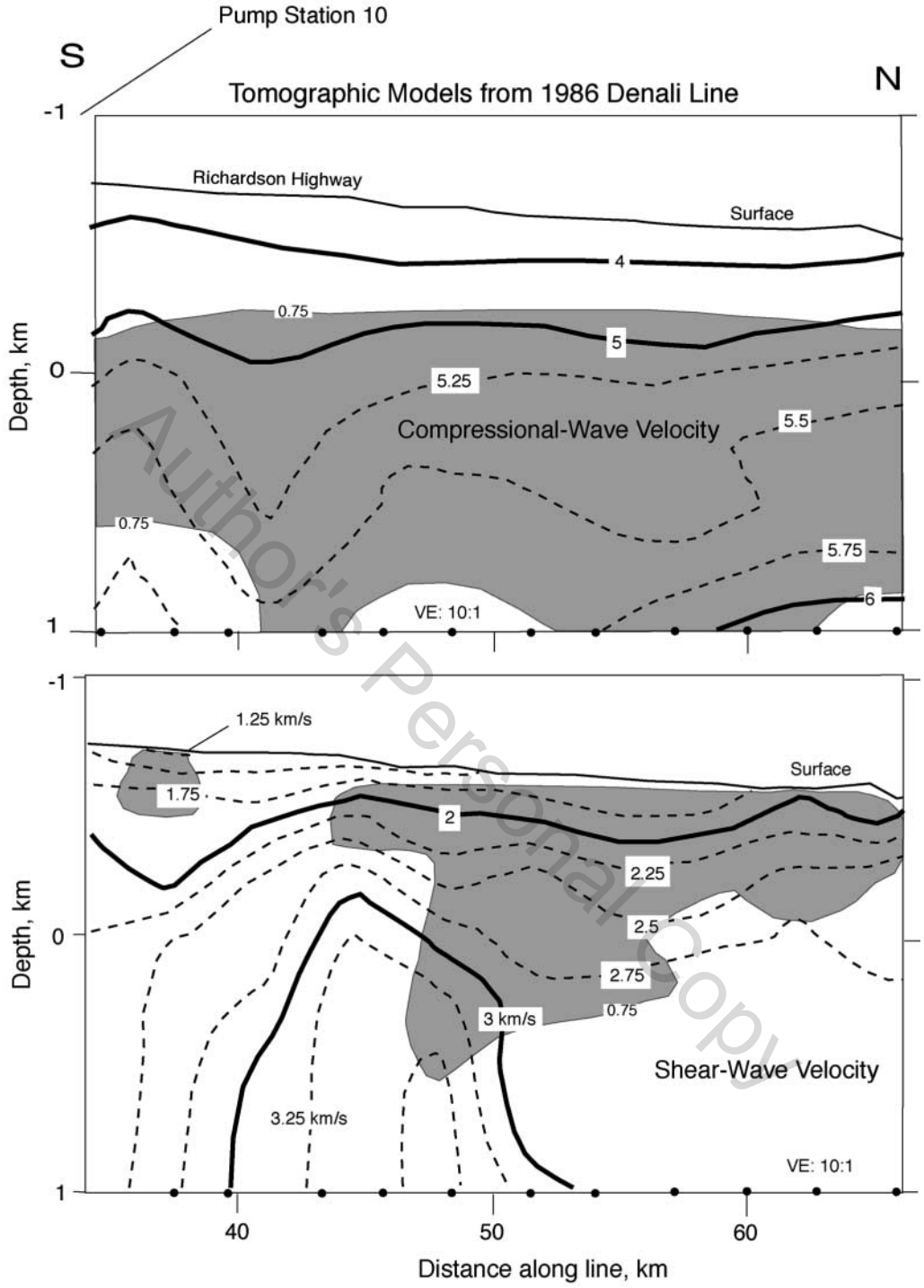

Figure 3. Comparison of tomography models for the TACT 1986 line for the (top) compressional and (bottom) shear-wave velocities in the shallow crust near the Trans-Alaska Pipeline Pump Station 10 (modified from Brocher *et al.*, 1991). Shaded regions correspond to better-resolved parts of the models (resolutions exceed 0.75). Dots along base of models show the horizontal location of the sources. Surficial V_s values of 1.2 to 1.8 km/sec are unrealistically high and result from undersampling of the surficial layer.

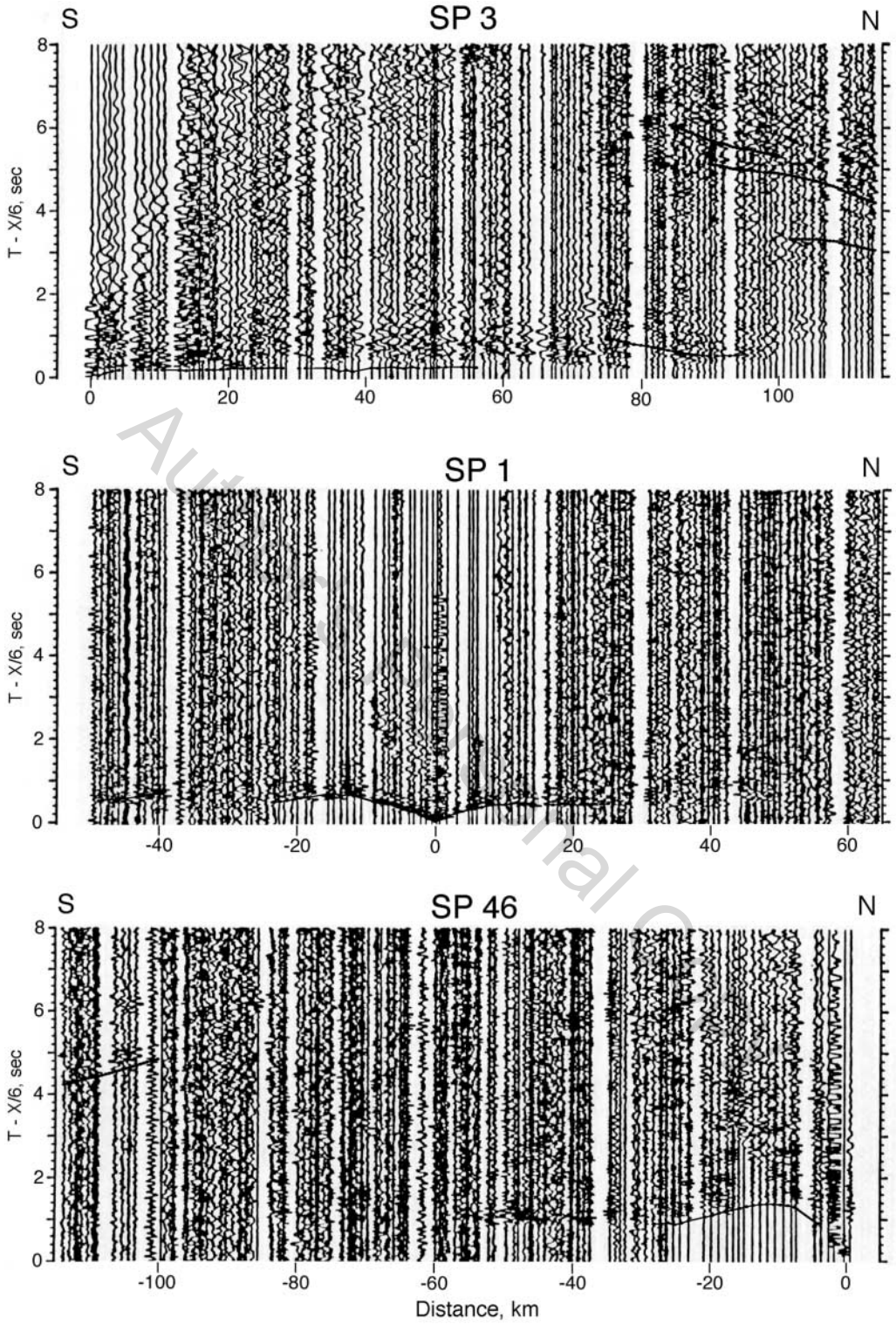

Figure 4. Three record sections from the TACT 1987 line illustrating data quality. The sections display refractions from the upper crust (*Pg*) and wide-angle reflections from the lower crust. Data are reduced to a velocity of 6 km/sec, and trace amplitudes are normalized. Note the general decline in data quality as the shot points move north. Black lines show travel times calculated from the velocity model in Figure 7.

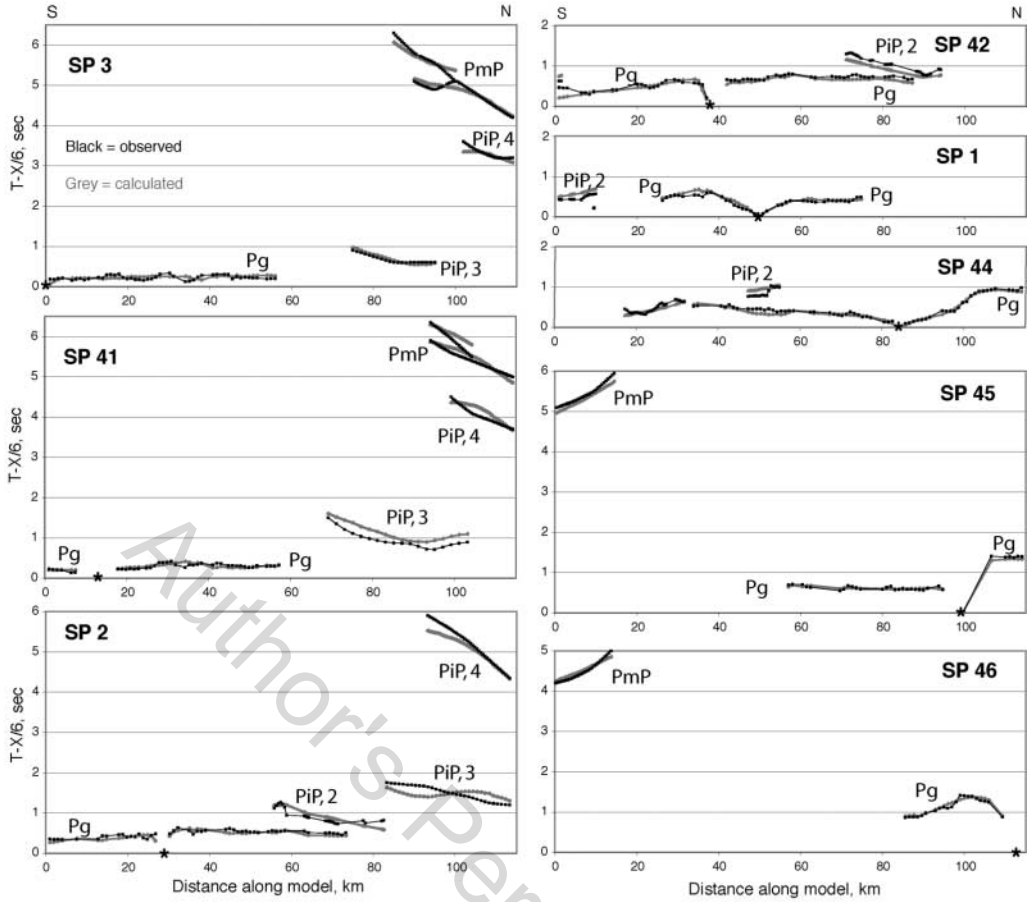

Figure 5. Comparison of observed and calculated travel times for the model given in Figure 7. The black asterisk indicates the model location of the shotpoint. Upper crustal refractions (*Pg*) and midcrustal reflections (*PiP*) labeled by their interface numbers (Fig. 7), and reflections from the Moho (*PmP*) are labeled. Note absence of reflections from deep interfaces from SP 42, SP 1, or SP 44.

only from shotpoints 49 and 54 located to the north of the line, with a crossover distance of about 160 km (Beaudoin *et al.*, 1989). These *Pn* arrivals yield an unreversed upper mantle velocity of 8.2 km/sec. Using $Z = 0.5X_{cr}((V_2 + V_1)/(V_2 - V_1))^{-0.5}$ for the relation between crossover distance, X_{cr}, and crustal thickness, Z (Sheriff and Geldart, 1995), with $V_1 = 6.4$ and $V_2 = 8.2$ km/sec, yields a crustal thickness of 28 km in the Yukon–Tanana terrane. By contrast, this relation and values predict a crustal thickness above 53 km from the data from Shotpoint (SP) 8 and SP 19, south of the line, which did not yield *Pn* arrivals out to distances of 300 km (Beaudoin *et al.*, 1989). Shear-wave arrivals were not prominent on the TACT 1987 record sections and were not used in our study.

Inversion of the TACT 1987 LINE

Two-dimensional velocity models for the TACT 1987 line were obtained from inversions of first- and second-arrival travel times. The line crossed the Denali and Hines Creek faults at oblique angles of 40° to 60°, and its interpretation should bear this obliquity in mind. A potential limitation of our model is its reliance on two-dimensional geometry. The receivers and shots closely followed the Richardson Highway, which curves gently (Fig. 1A). This curvature results in portions of the line lying as much as 5 km off the best-fitting linear projection to the line. We focus our discussion on results unlikely to be strongly influenced by this nonlinearity.

Upper Crustal Velocity Models

We inverted the first-arrival (*Pg*) travel times using a tomography algorithm described by Lutter *et al.* (1990). Velocities between nodes were interpolated using bicubic splines, so that no first-order velocity discontinuities were introduced into the model. We parameterized the model using 192 nodes spaced every 7.7 km in distance and every 0.6 km in depth on average (actual node depths were −2.0, −1.25, −1.0, −0.7, −0.4, −0.1, 0.5, 1.0, 1.5, 2.5, 4.5, and 7.0 km where 0.0 km is sea level). Although we tested models having more than 192 velocity nodes, their resulting

resolutions were judged to be unacceptably low, suggesting that 192 nodes sufficed.

One thousand rays at 0.3-km intervals were traced through the models, yielding a final average rms error of 0.063 sec for all 8 shots (Fig. 5). Table 1 lists the rms travel-time misfit for every shot (layer 1), indicating rms travel-time misfit range between 0.042 and 0.079 sec, comparable to or less than the accuracy of the travel time picks. The 348 first-arrival travel-time picks summarized in Table 1 represents the set of travel times used in the joint inversion for lower crustal structure described below: they are a subset of the 1000 picks available for the first-arrival-time tomography model.

Resolution and standard deviations of model parameters were calculated following Nowack and Lutter (1988) and Lutter *et al.* (1990). A linearized resolution matrix quantifies how our experimental geometry limits our ability to resolve the actual crustal velocity structure resulting in a smoother inverted crustal model. Diagonal elements of the resolution matrix range between values of 0 and 1 and are inversely proportional to the degree of averaging in the inverted model. Model parameters associated with diagonal elements of the resolution matrix greater than or equal to 0.5 have acceptable resolution values and are considered meaningful. The best-resolved portion of the model (model resolution 0.5 or more) lies less than 4 km below sea level (Fig. 6B), above a prominent electrical conductor and seismic reflector (Stanley *et al.*, 1990). The upper kilometer of the model was not as well resolved (Fig. 6B).

Lower Crustal Velocity Model

Velocities above interfaces and depths to five interfaces of the mid- to lower-crust (Fig. 7) were inverted from the travel times of wide-angle reflections from these horizons using an algorithm described by Lutter and Nowack (1990). The travel times for these second arrivals are illustrated in Figure 5. The depth to an interface and the velocity of the crust above the interface were simultaneously determined: the complete crustal model was obtained by working sequentially down through the crust, layer by layer. We inverted for a total of 20 parameters (velocity and interface nodes) for five interfaces, using 467 travel times, producing an acceptable average rms travel-time misfit of 0.12 sec for all five interfaces (Table 1).

Bicubic splines were used to interpolate points along the five interfaces. The velocities to a depth of 5.5 km below sea level were taken from the model derived from inversion of *Pg* travel times shown in Figure 6C. To start the inversion, we inverted reflection times for the velocities and thickness of the crust between 5.5- and 10-km depth. The best solution resulted in a layer with a negative velocity gradient with depth yielding velocities that decrease from 6.2 to 6.05 km/sec. We sequentially inverted for the velocity and thickness of all deeper layers. Our inversion produced a small velocity reversal (from 6.5 to 6.4 km/sec) at depths ranging between 18 and 40 km (Fig. 7). Only travel times from the 8 shots within the refraction profile were used in our inversion (Fig. 5), no travel times from off-end shots were analyzed.

Table 1 summarizes details of the interface inversion for every shot, including the number of wide-angle reflections used to invert for each interface. As many as 48 rays and as few as 13 rays were used at a single shot to constrain an interface. Each interface was sampled by as many as 146 and as few as 52 rays from all shotpoints. Figure 5 and Tables 1 and 2 indicate how each shot contributed reflection control on an interface. Nominal subsurface coverage provided by these reflections is summarized in Table 2, assuming horizontal interfaces. Because these interfaces dip gently, the subsurface coverage predicted by this table differs slightly from Figure 7.

Table 1 also summarizes the rms travel-time misfits for each interface and shot. Root mean square travel time misfits for individual shots range from a high of 0.205 sec (for interface 3) to a low of 0.050 sec (also for interface 3). For all shots, interface 3 had the largest average rms travel-time misfit.

Observed wide-angle reflection branches are short (Fig. 5), on the order of 10 to 20 km long, providing limited constraints on average crustal velocities and defining the geometry of interfaces only near the center of the profile (Fig. 7). Uncertainties in the velocities of the middle to lower

Table 1
Number of Rays and rms Travel Time Misfits (in sec) for Each Interface and Shotpoint

SP	SP (Model km)	Layer 1 (N, RMS)	Interface 2 (N, RMS)	Interface 3 (N, RMS)	Interface 4 (N, RMS)	Interface 5 (N, RMS)	Interface 6 (N, RMS)
3	0.00	46, 0.062	—	21, 0.050	25, 0.092	48, 0.085	30, 0.130
41	14.20	40, 0.046	—	18, 0.205	31, 0.139	41, 0.097	21, 0.171
2	28.33	48, 0.063	21, 0.117	31, 0.180	41, 0.178	—	—
42	37.77	59, 0.079	26, 0.131	—	—	—	—
1	49.65	42, 0.055	13, 0.119	—	—	—	—
44	84.70	60, 0.052	42, 0.094	—	—	—	—
45	99.46	32, 0.042	—	—	—	29, 0.109	—
46	113.71	21, 0.053	—	—	—	28, 0.075	—
All		348, 0.059	102, 0.113	70, 0.157	97, 0.148	146, 0.093	52, 0.147

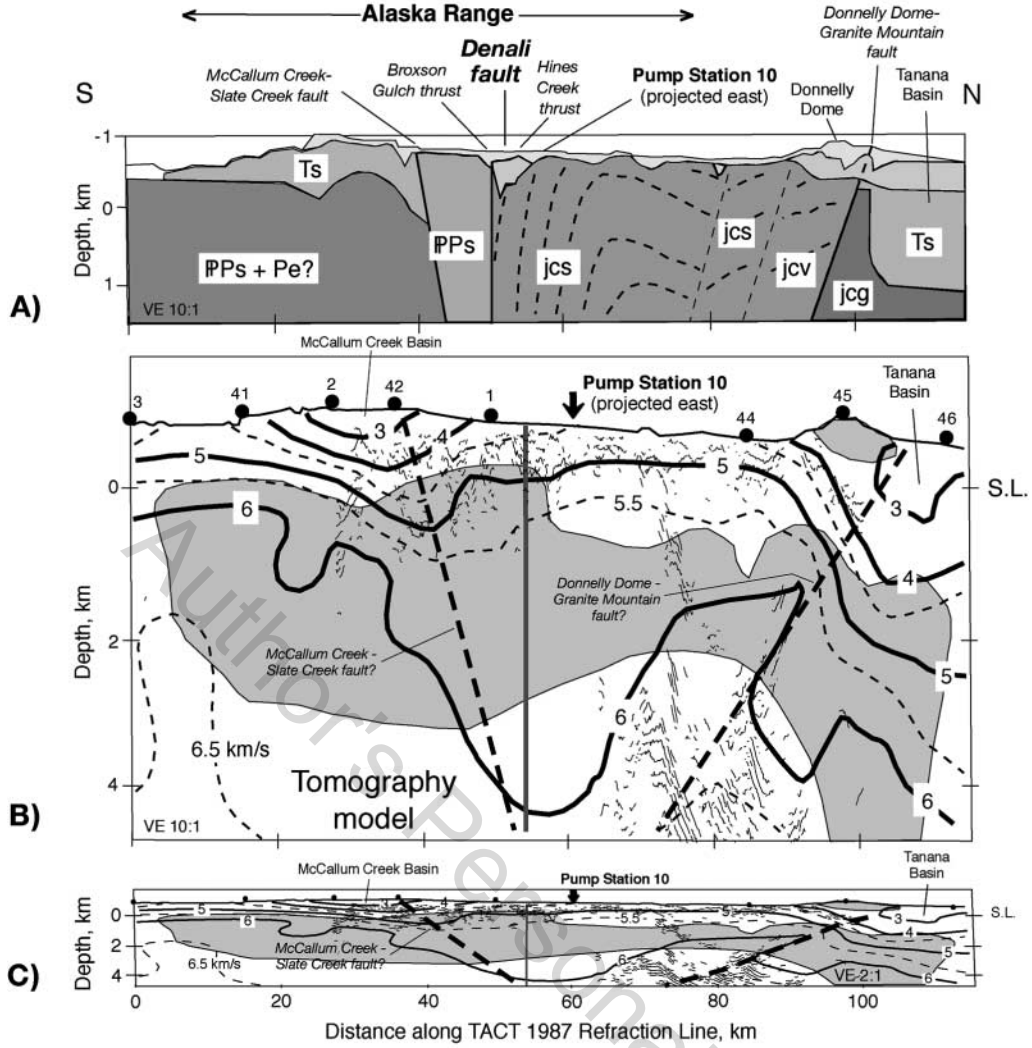

Figure 6. Tomography model for the TACT 1987 line. (A) Geologic cross section inferred from geologic mapping and shallow seismic refraction profiling (modified from Brocher *et al.*, 1991). *VE* = 10:1. Abbreviations for symbols used are as follows: jcs, Devonian and older metasedimentary rocks of the Jarvis Creek Glacier subterrane of the Yukon–Tanana terrane; jcv, Devonian metavolcanic rocks of the Jarvis Creek Glacier subterrane of the Yukon–Tanana terrane; jcg, Devonian metagranitic rocks of the Yukon–Tanana terrane; PPs, Pennsylvanian and Permian sedimentary and volcanic rocks of the Slana Spur Formation of the Wrangellia terrane; Pe, Permian sedimentary rocks of the Eagle Creek Formation of the Wrangellia terrane; Ts, Tertiary sedimentary rocks. (B) Tomography velocity model plotted with a vertical exaggeration of 10:1. Filled circles on top of the models show the location of shotpoints. Isovelocity lines are contoured at an interval of 0.5 km/sec. The gray shading highlights better-resolved parts of the model (resolutions greater than 0.5). Short lines indicate reflections from TACT 1986 seismic line presented by Fisher *et al.* (2004). (C) Same model as in part B plotted with less vertical exaggeration (VE 2:1)

crust range from 0.1 to 0.5 km/sec (Fig. 7). In particular, the 6.3 km/sec velocity of the layer between interfaces 5 and 6 at the base of the crust is poorly constrained, as indicated by a low resolution value of 0.25. The presence of a lower crustal layer that thins and terminates northward (between interfaces 5 and 6) is inferred from two wide-angle reflections that converge northward. The velocity within this layer, 6.3 ± 0.5 km/sec, however, is poorly constrained. In Figure 7, we show this layer as terminating north of the southern end of our line as the layer is not reported to the south of our line (Fuis *et al.*, 1991).

The depth to the Moho generally has an uncertainty of about ±10%, or ±5 km in our study area. The strongly concave geometry of the interfaces below 20-km depth results from the bicubic spline used to interpolate points along the interfaces.

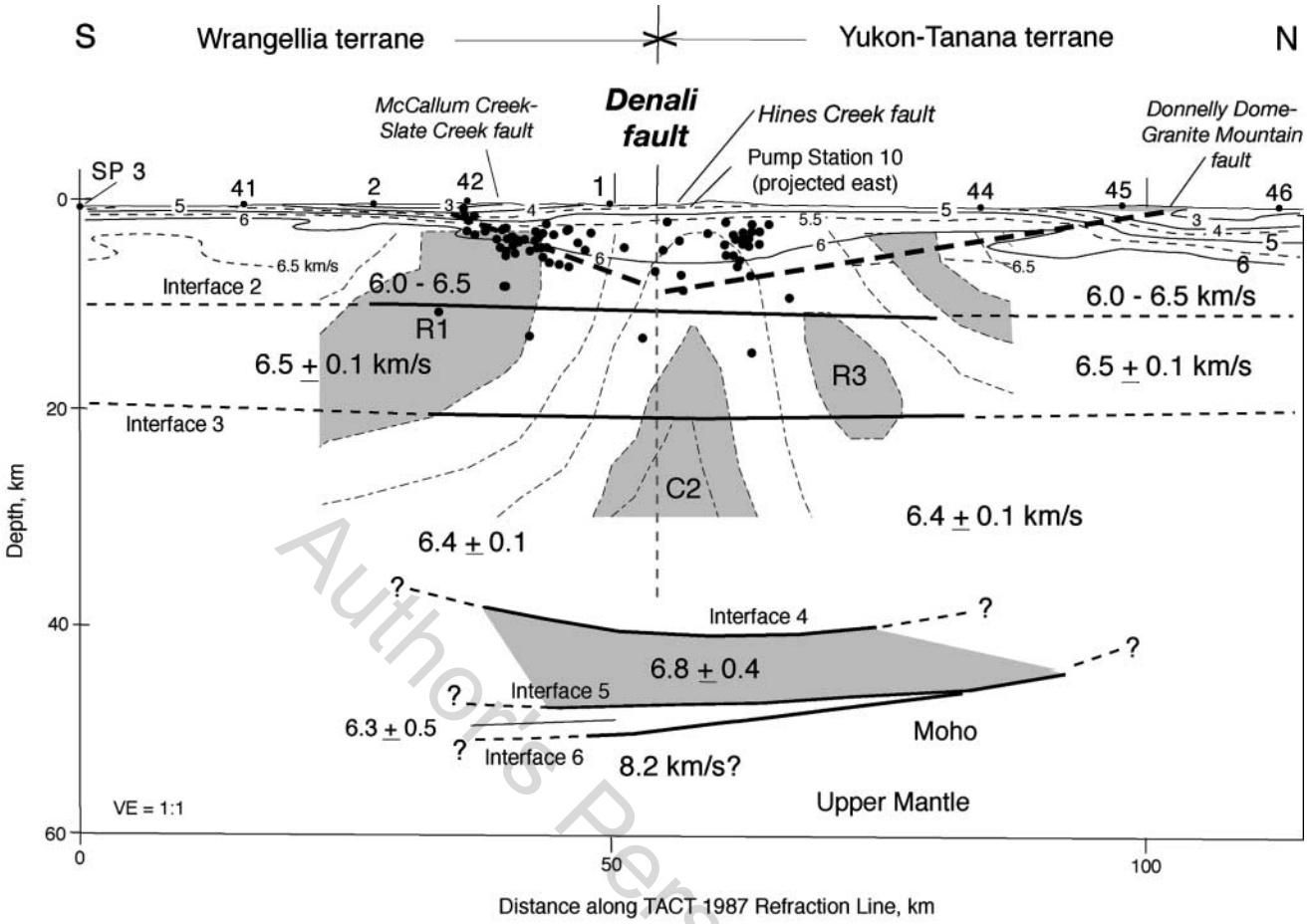

Figure 7. Velocity model for the TACT 1987 line. Velocities in the upper 5 km are taken from Figure 6B. Shotpoint locations are provided at the top of the model. Solid lines along interfaces indicate locations of reflection points. Dashed lines along interfaces are not constrained by reflections and are projected. High electrical resistivity units R1, R3, and R4 and high conductivity unit C2, from Fisher *et al.* (2004), are shaded in gray. Aftershocks of the Denali fault earthquake plotted as small solid dots. Thick dashed lines represent inferred thrust faults (Donnelly Dome–Granite Mountain and McCallum Creek–Slate Creek).

Table 2
Nominal Midpoints of Reflections from Interfaces, Assuming Horizontal Layers

SP	SP (Model km)	Midpoints Interface 2 Model km)	Midpoints Interface 3 Model km)	Midpoints Interface 4 Model km)	Midpoints Interface 5 Model km)	Midpoints Interface 6 Model km)
3	0.00	—	38–48	51–57	45–57	43–50
41	14.20	—	42–59	57–64	54–64	54–59
2	28.33	42–56	56–71	61–71	—	—
42	37.77	20, 55–66	—	—	—	—
1	49.65	25–30	—	—	—	—
44	84.70	51–58, 66–70	—	—	—	—
45	99.46	—	—	—	50–57	—
46	113.71	—	—	—	57–64	—
All		20, 25–30, 42–70	38–71	51–71	45–64	43–59

Results

Cenozoic Basins

The *P*-wave velocity isocontour of 5 km/sec from the TACT 1987 line coincides with the base of shallow seismic reflectivity along the TACT 1986 line (Fig. 6B). A velocity of ~5 km/sec is an approximate upper limit for the velocities of Cenozoic sedimentary rocks in Alaska (Fuis *et al.*, 1991). Combined with the base of reflectivity, this isovelocity contour provides an approximate estimate for the maximum thickness of Tertiary sedimentary basin fill. Two thin sedimentary basins along the line are identified, one in the Alaska Range (McCallum Creek basin) and one in the Delta Junction area (Tanana basin). The McCallum Creek basin appears to be ~1.5 km thick, and the Tanana basin appears to be ~3 km thick.

Fig. 8 compares our velocity model with coincident isostatic gravity anomalies. In isostatic gravity maps (e.g., Morin and Glen, 2003) both the McCallum Creek and Tanana basins are associated with pronounced gravity anomaly lows typical of significant thicknesses of Cenozoic sedimentary rocks having a large density contrast with the underlying basement rocks. The McCallum Creek basin is delineated as an elongate, northwest-trending isostatic gravity low about 28 km long and 18 km wide (Morin and Glen, 2003). These maps indicate that the TACT 1987 line traversed the center and deepest part of that basin. Similar isostatic gravity maps indicate that the TACT 1987 line traversed the easternmost and narrowest part of a segment of the northwest-trending Yukon–Tanana basin (not shown).

Upper Crustal Basement Rocks

In agreement with the TACT 1986 line results (Brocher *et al.*, 1991), the TACT 1987 model (Fig. 6B) shows relatively high surficial velocities for Yukon–Tanana terrane basement rocks, which crop out between model ranges of 60 and 100 km. The model provides evidence for a slight northward shallowing of the *P*-wave velocity isocontours within the Yukon–Tanana terrane (Fig. 6B), consistent with a northward increase in the seismic velocity. As did Brocher *et al.* (1991), we attribute this northward increase to (1) the intrinsic anisotropy of these mica-quartz schists, in which velocities are fast parallel to the foliation and slower perpendicular to the foliation, coupled with (2) the systematic northward decrease in the dip of foliation (Fig. 6A); together, (1) and (2) produce progressively faster rock to the north, in the direction of horizontally propagating refractions.

Denali Fault Zone

The tomography model for the TACT 1987 line indicates that the Denali fault zone is associated with lower velocities (note the depression in 6 km/sec contour) as is expected for a major, active strike-slip fault (Mooney and Ginzburg, 1986). The 40-km width of the low-velocity zone, however, is 10 to 20 times wider than observed along other fault zones

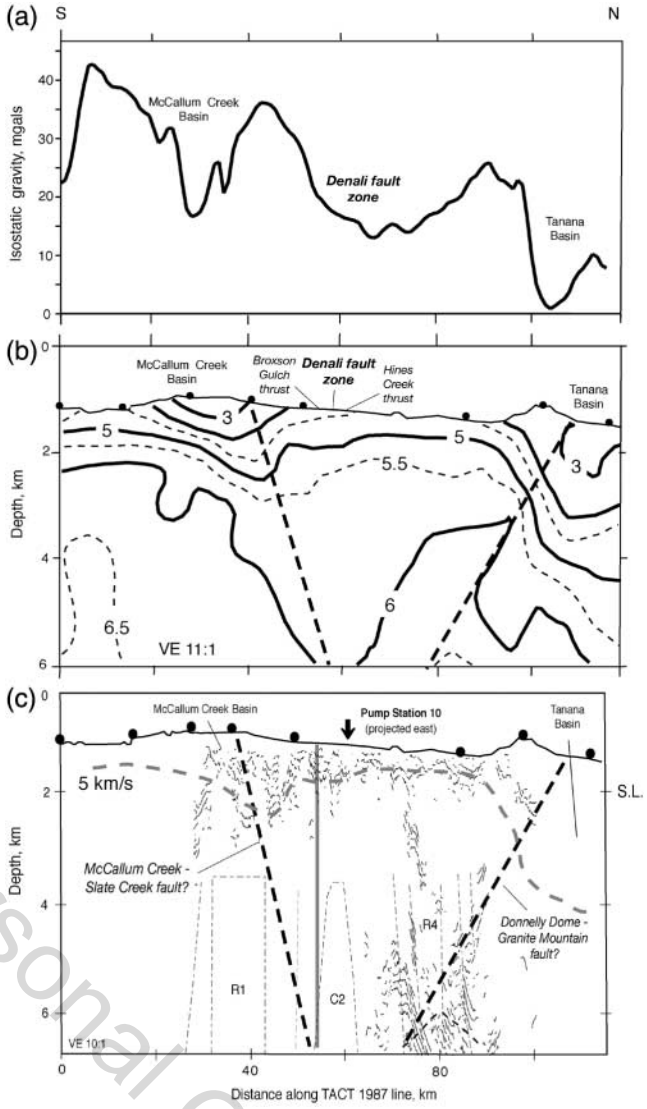

Figure 8. (a) Isostatic gravity anomalies (Morin and Glen, 2003), (b) velocity model for the TACT 1987 line (from Fig. 6B), and (c) seismic reflectivity from the TACT 1986 line (Fisher *et al.*, 2004).

(although as much as half of this apparent width could result from the strong obliquity of the seismic line to the fault zone). As described below, we believe this excessive width results from the composite damage associated with several strands of the Denali fault zone.

The Denali fault zone is associated with subdued isostatic gravity low whose location and width seem best correlated with the geometry of the 6 km/sec isocontour (Fig. 8A). The 20-km-wide gravity low along the Denali fault zone is traceable using sparse gravity observations for about 70 km west of the Richardson Highway (Morin and Glen, 2003) but is not apparent to the east of the highway. We attribute the general northward decrease in the isostatic gravity (Fig. 8A) to northward deepening of the depth to top of basement as indicated by the 5 km/sec isocontour.

McCallum Creek–Slate Creek and Donnelly Dome–Granite Mountain Faults

Upward steps in the 4.5, 5, and 5.5 km/sec contours between the 40- and 60-km model range, within and north of the McCallum Creek basin, are offset progressively northward with depth, suggesting the possibility of a shallowly northward-dipping thrust fault. We have tentatively interpreted these contour shapes as evidence of the northward extension of the McCallum Creek–Slate Creek thrust fault. This interpretation is also supported by the velocity model for TACT 1986 (Fig. 2).

Sharp upward ramps and steps in the 3 to 6 km/sec contours beneath and south of Donnelly Dome are offset progressively southward with depth, suggesting the possibility of a shallowly southward-dipping thrust fault. We interpret these contour shapes as evidence of the southward extension of the Donnelly Dome-Granite Mountain thrust fault.

Moho Geometry

Our velocity model is consistent with a crustal thickness of about 50 km and with northward thinning of the crust (Fig. 7). Forward modeling of travel times of wide-angle reflections from the Moho (*PmP*) suggests a crustal thickness of 52 km beneath the Wrangellia terrane. For shotpoints within the Wrangellia terrane (SP 3 and SP 41) on the southern end of the line, *PmP* reflections are emergent, suggesting the presence of a several-kilometer-thick transition from crustal velocities to upper mantle velocities (between interfaces 5 and 6, see Fig. 7). On the northern half of the line, for shotpoints in the Yukon–Tanana terrane (SP 45 and SP 46), *PmP* reflections are more prominent, suggesting a thinner transition zone between crustal and upper mantle velocities. The best constraints on the crustal thickness within the Yukon–Tanana terrane to the north of the TACT 1987 line are provided by a refraction line described by Beaudoin *et al.* (1992); (the location of this line is shown in Fig. 1A). Beaudoin *et al.* (1992) show that the crust at the northern end of our profile is between 28 and 30 km thick (Fig. 7).

Discussion

Pump Station 10

Trans-Alaska Pipeline Pump Station 10 is located about 300 m west of the TACT 1986 line, placing it closer to the Delta River than to the seismic line. Based on Figures 2 and 3, the Quaternary deposits and weathered bedrock at the Pump Station are a total of about 70 m thick. These deposits directly overlie Yukon–Tanana terrane schists having significantly higher compressional-wave seismic velocities (Fig. 2A), as required by the abrupt change in the slope of the first arrivals (Brocher *et al.*, 1991). Projecting contours in the shear-wave velocity model for the TACT 1986 line (Fig. 3) southward by about 300 m allows us to summarize the compressional- and shear-wave velocity structure at the station (Table 3). *S*-wave velocities below 5 km depth in Table 3 were calculated from the *P*-wave velocity assuming a V_p/V_s ratio of 1.73 (see Tables 4–6), close to that inferred near Fairbanks (Fig. 1A) from teleseismic receiver function analysis (Searcy *et al.*, 1996).

Table 3
1D Velocity Model for Pump Station 10

Depth (km)	V_p (km/sec)	V_s (km/sec)
0.00	1.70	0.62†
0.07	1.90	0.75
0.07	4.90	2.00
0.90	5.30	2.10
0.90	5.50	3.18
5.00	6.00	3.47*
10.00	6.50	3.76*
20.00	6.50	3.76*
20.00	6.40	3.70*
40.00	6.40	3.70*
40.00	6.80	3.93*
47.00	6.80	3.93*
47.00	6.30	3.64*
50.00	6.30	3.64*
50.00	8.20	4.74*
60.00	8.20	4.74*

*Assumed $V_p/V_s = 1.73$.
†Kayen *et al.* (2004) reported an average V_s in the upper 30 m of 0.32 km/sec.

Ellsworth *et al.* (2004) inferred an International Building Code 2003 (IBC2003) type D soil for Pump Station 10 based on spectral analysis of surface wave (SASW) shear-wave velocities (Kayen *et al.*, 2004), coarse-grained lithologies, and blow counts. SASW measurements at Pump Station 10 yielded an average shear-wave velocity of 316 m/sec in the first 30 m and shear-wave velocities in excess of 600 m/sec at a depth of 115 m (Kayen *et al.*, 2004), or about half those reported by Brocher *et al.* (1991) and given in Table 3. Given the 3-km shot spacing used in their study, however, Brocher *et al.* (1991) had limited resolution in the upper hundred meters.

Recorded accelerations from the Denali fault earthquake were largest at Pump Station 10 simply because this site was located closest to the earthquake and in the direction of rupture propagation (Ellsworth *et al.*, 2004; Frankel, 2005). However, did the local crustal structure increase strong ground motions there? Pump Station 10 lies within the broad zone of lower velocities associated with the fault zone extending to 5-km depth (Fig. 6B), which may channel seismic energy along the fault. Nonetheless, Pump Station 10 lies outside the narrow band of lower velocities (Fig. 2) inferred to represent intense fault damage along the Denali fault zone expected to significantly increase ground motions (e.g., Li *et al.*, 1990, 1994, 1995, 1997). From its location outside of the damage zone we infer that only weak focusing of strong motions at the location of Pump Station 10 resulted from the known crustal structure.

Table 4
Laboratory Measurements of Gulkana River Complex and Wrangellia Terrane Rocks

Press (MPa)	TA-14	TA-15	TA-16	TA-27	TA-17	TA-18	TA-19	TA-22	TA-28	Average
					P-Wave Velocity (km/sec, Mean Values)					
10	6.694	6.248	5.374	5.646	5.704	6.617	6.947	4.991	5.687	5.990
50	6.784	6.613	5.708	5.951	5.986	6.741	7.132	5.426	6.042	6.265
100	6.814	6.790	5.886	6.081	6.095	6.802	7.217	5.662	6.178	6.392
200	6.871	6.937	6.049	6.195	6.177	6.869	7.308	5.865	6.276	6.505
400	6.933	7.051	6.173	6.302	6.250	6.938	7.399	6.002	6.361	6.601
600	6.971	7.108	6.232	6.363	6.293	6.978	7.448	6.065	6.409	6.652
800	6.999	7.147	6.272	6.406	6.324	7.003	7.480	6.107	6.441	6.687
1000	7.020	7.177	6.304	6.439	6.347	7.021	7.503	6.138	6.465	6.713
					S-Wave Velocity (km/sec, Mean Values)					
10	3.946	3.643	3.304	3.417	3.558	3.766	4.044	3.000	3.420	3.566
50	4.004	3.772	3.466	3.530	3.681	3.817	4.129	3.200	3.499	3.678
100	4.030	3.829	3.551	3.587	3.736	3.842	4.167	3.294	3.538	3.730
200	4.054	3.879	3.613	3.646	3.770	3.868	4.203	3.376	3.576	3.776
400	4.077	3.923	3.648	3.699	3.792	3.893	4.235	3.444	3.610	3.813
600	4.090	3.944	3.664	3.727	3.803	3.904	4.252	3.478	3.626	3.832
800	4.100	3.959	3.676	3.745	3.812	3.911	4.264	3.499	3.636	3.845
1000	4.107	3.970	3.685	3.760	3.818	3.915	4.272	3.515	3.643	3.854
					V_p/V_s Ratio (Mean Values)					
10	1.696	1.715	1.627	1.652	1.603	1.757	1.718	1.664	1.663	1.677
50	1.719	1.815	1.728	1.742	1.682	1.790	1.764	1.809	1.727	1.753
100	1.702	1.800	1.698	1.723	1.656	1.782	1.748	1.769	1.746	1.736
200	1.705	1.812	1.703	1.727	1.653	1.788	1.754	1.781	1.755	1.742
400	1.710	1.818	1.709	1.728	1.658	1.794	1.760	1.778	1.762	1.746
600	1.710	1.812	1.708	1.720	1.660	1.792	1.759	1.761	1.768	1.743
800	1.711	1.812	1.712	1.719	1.663	1.794	1.759	1.756	1.771	1.744
1000	1.712	1.813	1.715	1.719	1.665	1.795	1.760	1.754	1.775	1.745
					Poisson's Ratio (Mean Values)					
10	0.234	0.242	0.196	0.211	0.182	0.260	0.244	0.217	0.217	0.223
50	0.244	0.282	0.248	0.254	0.227	0.273	0.263	0.280	0.248	0.258
100	0.236	0.277	0.235	0.246	0.213	0.270	0.257	0.265	0.256	0.251
200	0.238	0.281	0.237	0.248	0.212	0.272	0.259	0.270	0.260	0.253
400	0.240	0.283	0.239	0.248	0.214	0.275	0.262	0.269	0.262	0.255
600	0.240	0.281	0.239	0.245	0.215	0.274	0.261	0.262	0.265	0.254
800	0.241	0.281	0.241	0.244	0.217	0.275	0.261	0.260	0.266	0.254
1000	0.241	0.281	0.242	0.244	0.218	0.275	0.261	0.259	0.267	0.254
Density (kg/m^3)	3088	3048	2624	2671	2823	3011	3154	2587	2771	2864

Brocher *et al.* (1991); N. I. Christensen (unpublished data, 2003).

Denali Fault Zone

The TACT 1986 and 1987 lines provide velocity models having different spatial and depth resolution of the Denali fault zone. The higher resolution TACT 1986 line images a narrow, 5-km-wide, low-velocity zone (lvz) centered on the Denali fault zone (Fig. 1). This narrow and shallow (<400 m deep) lvz is attributed to fault zone damage along the Denali and nearby thrust faults (Broxson Gulch and Hines Creek thrusts). Given the 3-km source spacing used for this model, we cannot rule out the possibility that a narrow (<500 m wide) lvz along the near-vertical Denali fault zone persists to greater depths than depicted in Figure 2.

The lower-resolution but deeper-penetrating TACT 1987 line images a 40-km-wide velocity low, best seen in the 6 km/sec isocontour, centered just north of the Denali fault zone (Fig. 8). Reduced *P*-wave velocities in this broad lvz (Fig. 8B) probably result from the shearing and fracturing of large volumes of rock during strike-slip and dip-slip faulting along several strands of the Denali fault zone. This low-velocity zone is too broad to have formed along a single fault strand, since studies of low velocity zones along other strike-slip faults find widths less than 2 km (Mooney and Ginzburg, 1986; Li *et al.*, 1990, 1994, 1995, 1997; Chester *et al.*, 1999; Spudich and Olsen, 2001). Obliquity of the seismic line to the Denali fault zone contributes to up to half of this apparent 40-km width. Nonetheless, the inferred 20-km-wide fault zone would still be 10 times larger than observed elsewhere along other single fault strands. Well-known horizontal smearing by the tomography method is

Table 5
Laboratory Measurements of Yukon–Tanana Terrane Rocks Located within TACT 1987 Line

Press (MPa)	TA-20	TA-21	TA-29	TA-115	TA-114	TA-112	TA-113	Average
				P-Wave Velocity (km/sec Mean Values)				
10	4.431	4.274	5.802	5.367	5.536	5.691	5.628	5.247
50	5.482	5.240	6.198	5.774	5.915	5.935	5.864	5.773
100	5.886	5.710	6.311	5.950	6.049	6.038	5.975	5.988
200	6.073	5.998	6.383	6.076	6.151	6.136	6.077	6.128
400	6.160	6.136	6.445	6.178	6.245	6.236	6.168	6.224
600	6.203	6.202	6.479	6.237	6.301	6.297	6.219	6.277
800	6.232	6.247	6.501	6.279	6.340	6.342	6.254	6.314
1000	6.252	6.280	6.517	6.312	6.371	6.376	6.282	6.341
				S-Wave Velocity (km/sec Mean Values)				
10	3.187	2.740	3.503	3.124	3.244	3.331	3.362	3.213
50	3.593	3.316	3.620	3.325	3.385	3.442	3.484	3.452
100	3.789	3.646	3.674	3.418	3.451	3.496	3.541	3.574
200	3.898	3.880	3.713	3.490	3.510	3.542	3.584	3.660
400	3.938	3.975	3.738	3.546	3.562	3.578	3.617	3.708
600	3.954	4.001	3.749	3.578	3.590	3.597	3.635	3.729
800	3.963	4.016	3.755	3.600	3.610	3.611	3.648	3.743
1000	3.969	4.026	3.759	3.618	3.625	3.622	3.658	3.754
				V_p/V_s Ratio (Mean Values)				
10	1.390	1.560	1.656	1.718	1.707	1.708	1.674	1.631
50	1.720	1.912	1.712	1.737	1.747	1.724	1.683	1.748
100	1.638	1.722	1.718	1.741	1.753	1.727	1.687	1.712
200	1.603	1.645	1.719	1.741	1.752	1.732	1.696	1.698
400	1.580	1.581	1.724	1.742	1.753	1.743	1.705	1.690
600	1.575	1.560	1.728	1.743	1.755	1.751	1.711	1.689
800	1.576	1.561	1.731	1.744	1.756	1.756	1.714	1.691
1000	1.578	1.564	1.734	1.745	1.758	1.760	1.717	1.694
				Poisson's Ratio (Mean Values)				
10	−0.036	0.151	0.213	0.244	0.239	0.239	0.223	0.182
50	0.245	0.312	0.241	0.252	0.257	0.247	0.227	0.254
100	0.203	0.246	0.244	0.254	0.259	0.248	0.229	0.240
200	0.181	0.207	0.244	0.254	0.259	0.250	0.233	0.233
400	0.166	0.167	0.247	0.254	0.259	0.255	0.238	0.226
600	0.162	0.151	0.248	0.255	0.260	0.258	0.241	0.225
800	0.163	0.152	0.250	0.255	0.260	0.260	0.242	0.226
1000	0.164	0.154	0.251	0.255	0.261	0.262	0.243	0.227
Density (kg/m^3)	2645	2633	2751	2703	2761	2735	2680	2701

Brocher *et al.* (1991); N. I. Christensen (unpublished data, 2003).

unlikely to cause this large lvz width, due to the close correspondence between the shape of the gravity anomaly (Fig. 8A), and the geometry of the 6 km/sec isocontour (Fig. 8B). We do not attribute the lowering of the compressional-wave velocities in this zone as being related to shear heating resulting from earthquake rupture because temperature coefficients of -0.5 to -0.6×10^{-3} km/sec/C° for typical rock types in the shallow crust (Christensen, 1979) would require temperatures along the shallow fault zone to be elevated by several hundred C°.

Our tomography model from the TACT 1987 line loses resolution at depths more than 6 km (Fig. 6B). Thus, we cannot rule out the possibility that a narrow (<500 m wide) lvz lies along the near vertical fault to greater depth.

The spatial location of this broad lvz coincides with that of the electrically high conductivity unit, C2, reported by Fisher *et al.* (2004). Fisher *et al.* (2004) argued that the C2 anomaly images the Denali fault zone as a nearly vertical structure down to 30-km depth (Fig. 7). Altogether, these observations suggest that the Denali fault zone can be geophysically imaged throughout much of the crust and that it is nearly vertical. These geophysical lows are centered on the Hines Creek fault strand of the Denali fault zone. Inversion of GPS data for the coseismic slip from the Denali fault earthquake is also consistent with a slip on a high-angle, 85°-dipping fault (Hreinsdottir *et al.*, 2003). We are unaware of any other seismic lines crossing the Denali fault zone in other places to which our model can be compared.

Table 6
Laboratory Measurements of Yukon–Tanana Terrane Rocks Located North of TACT 1987 Line

Press (MPa)	TA-42	TA-47	TA-45	TA-46	TA-44	TA-43	TA-56	TA-57	Average
				P-Wave Velocity (km/sec, Mean Values)					
10	5.139	5.739	5.985	5.344	4.810	5.155	5.346	4.401	5.240
50	5.534	5.868	6.082	5.609	5.196	5.477	5.730	4.917	5.552
100	5.731	5.932	6.132	5.738	5.397	5.628	5.886	5.194	5.705
200	5.894	6.003	6.191	5.862	5.602	5.764	6.026	5.436	5.847
400	6.019	6.075	6.260	5.976	5.786	5.887	6.160	5.611	5.972
600	6.084	6.115	6.304	6.039	5.882	5.957	6.235	5.697	6.039
800	6.129	6.142	6.335	6.083	5.949	6.006	6.289	5.758	6.086
1000	6.164	6.162	6.359	6.117	6.002	6.043	6.331	5.806	6.123
				S-Wave Velocity (km/sec, Mean Values)					
10	3.079	3.497	3.520	3.170	2.810	3.267	3.063	2.749	3.144
50	3.286	3.562	3.554	3.301	3.041	3.452	3.222	3.074	3.312
100	3.394	3.594	3.576	3.376	3.171	3.551	3.306	3.254	3.403
200	3.479	3.619	3.603	3.440	3.306	3.639	3.386	3.429	3.488
400	3.534	3.637	3.629	3.482	3.423	3.704	3.452	3.567	3.554
600	3.561	3.646	3.643	3.500	3.479	3.735	3.485	3.636	3.586
800	3.580	3.652	3.653	3.512	3.516	3.756	3.508	3.683	3.608
1000	3.595	3.657	3.659	3.521	3.544	3.773	3.525	3.721	3.624
				V_p/V_s Ratio (Mean Values)					
10	1.669	1.641	1.700	1.686	1.712	1.578	1.745	1.601	1.667
50	1.684	1.647	1.711	1.699	1.709	1.587	1.778	1.600	1.677
100	1.689	1.651	1.715	1.700	1.702	1.585	1.780	1.596	1.677
200	1.694	1.659	1.718	1.704	1.694	1.584	1.780	1.585	1.677
400	1.703	1.670	1.725	1.716	1.690	1.589	1.784	1.573	1.681
600	1.709	1.677	1.730	1.725	1.691	1.595	1.789	1.567	1.685
800	1.712	1.682	1.734	1.732	1.692	1.599	1.793	1.563	1.688
1000	1.715	1.685	1.738	1.737	1.694	1.602	1.796	1.560	1.691
				Poisson's Ratio (Mean Values)					
10	0.220	0.205	0.236	0.229	0.241	0.164	0.256	0.180	0.216
50	0.228	0.208	0.241	0.235	0.240	0.170	0.269	0.179	0.221
100	0.230	0.210	0.242	0.235	0.236	0.169	0.270	0.177	0.221
200	0.233	0.215	0.244	0.237	0.233	0.169	0.269	0.170	0.221
400	0.237	0.221	0.247	0.243	0.231	0.172	0.271	0.161	0.223
600	0.239	0.224	0.249	0.247	0.231	0.176	0.273	0.156	0.225
800	0.241	0.227	0.251	0.250	0.232	0.179	0.274	0.154	0.226
1000	0.242	0.228	0.253	0.252	0.232	0.181	0.275	0.151	0.227
Density (kg/m^3)	2644	2624	2768	2641	2633	2615	2755	2531	2651

Beaudoin *et al.* (1992); N. I. Christensen (unpublished data, 2003).

Subsurface Geometry of Thrust Faults

Maps of aftershocks of the 2002 Denali fault earthquake show that relatively few aftershocks occurred in the immediate vicinity of the Richardson Highway (Fig. 1B). For that reason we have plotted cross sections of the aftershocks not only along the Richardson Highway, but also to the west and east of the highway where the aftershock sequence was more vigorous (Fig. 9). The cross section width is 20 km, that is to say, 10 km on each side of the section. Along and to the east of the highway, these cross sections define a shallow, north-dipping plane of aftershocks between depths of 7 km and the surface. Along the Richardson Highway these aftershocks define a plane dipping about 26° to the north, bounded on the north by the Denali fault zone (Fig. 9). Thus they appear to be associated with a shallow, north-dipping thrust fault that ruptures the surface, most likely the McCallum Creek–Slate Creek fault.

Our velocity model images a similar shallowly north-dipping Donnelly Dome–Granite Mountain thrust fault (Fig. 6A). This fault, marking the northern boundary of the Alaska Range, is a north side upthrust having a major (20–60 m high) north-facing escarpment in late Wisconsin deposits (Hudson and Weber, 1977). We infer that this fault is bounded to the south by the Denali fault zone.

The north-dipping McCallum Creek–Slate Creek and south-dipping Donnelly Dome–Granite Mountain faults (Rose, 1967; Hudson and Weber, 1977) appear to define a

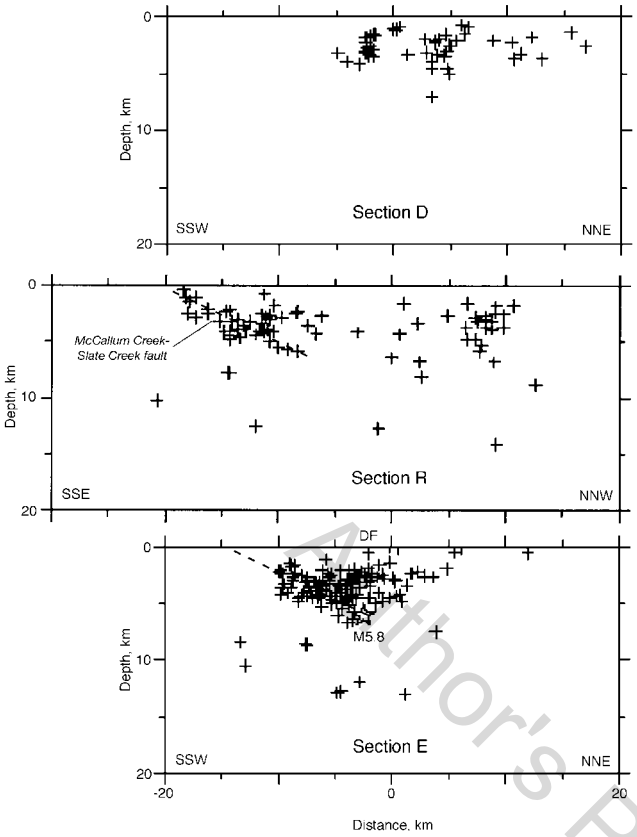

Figure 9. Aftershocks of the 2002 Denali fault earthquake plotted as plus symbols for three sections crossing the Denali fault (locations of sections provided in Fig. 1B). Sections D and E, respectively located west and east of the Richardson Highway, are from Ratchkovski *et al.* (2003). Section R is located along the Richardson Highway.

large flower structure (Harding, 1985) associated with the Denali fault zone. Rose (1967) mapped a narrow, thin (~300 m), fault-bounded block of Tertiary sedimentary rocks within the Slate Creek fault zone, which he identified as a right-lateral fault with a steep northward dip. The north-dipping Broxson Gulch thrust and the south-dipping Hines Creek fault probably represent additional thrust faults in this larger flower structure. Within our study area, the Broxson Gulch thrust is mapped as a narrow zone of imbricate thrusts dipping northward between 5° and 40° (Stout and Chase, 1980). The right-lateral strike-slip Hines Creek fault dips steeply southward and has evidence for a significant thrust component (Nokleberg *et al.*, 1989). Presumably these thrusts merge downward at depth, forming a narrower fault system at depth than is observed at the surface.

Relationships among Seismic Velocity, Electrical Resistivity, and Seismic Reflectivity in the Middle Crust

There are a number of intriguing relationships between the velocity, resistivity, and reflectivity models. The upper boundaries of highly electrically resistive units, R1 and R4, identified by Fisher *et al.* (2004), correspond to *P*-wave velocities greater than 6 km/sec (Figs. 6B, 7). Whereas the isolated resistive unit R3 lies nearly entirely within the 6.5 ± 0.1 km/sec layer between 10 and 20 km depth, unit R1 is not confined to any velocity layer but extends vertically across layer boundaries (Fig. 7). The midcrustal set of reflections north of the Denali fault zone (Fig. 6, feature B); (see Fisher *et al.*, 2004) lies almost entirely within the 6.5 ± 0.1 km/sec layer between 10 and 20 km depth. The truncation of the B reflectivity at or near 20-km depth is associated with a decrease in *P*-wave velocity from 6.5 to 6.4 km/sec (Fig. 7).

Composition of the Middle and Lower Crust

Average crustal velocities in the Alaska Range at 10- to 40-km depths are relatively low in comparison to typical continental crust (Christensen and Mooney, 1995), between 6.4 and 6.5 km/sec (Fig. 7). These refraction velocities are comparable to laboratory measurements of compressional-wave velocity (Tables 4–8) measured for many suites of samples along the TACT line (Fig. 10). These measurements indicate that on average, velocities decrease northward along the TACT line, with the highest velocities being found in the metamorphic complex of Gulkana River and the Wrangellia terrane (Table 4). Rocks in the southernmost part of the Yukon–Tanana terrane have intermediate velocities (Table 5) and rocks in the central and northern Yukon–Tanana terrane are the most felsic and have the lowest velocities (Table 6). Table 8 presents measurements for samples from west of the transect of the Kahiltna Formation, proposed to have been thrust beneath the Yukon–Tanana terrane (Stanley *et al.*, 1990). Tables 4–6 also summarize the shear-wave velocities, V_p/V_s, and Poisson's ratios of these samples.

Comparison of the laboratory and refraction seismic velocities (Fig. 10) suggests that the midcrust along the TACT 1987 line might be composed of a wide variety of rock types. The measurements are inconsistent, however, with a midcrust composed almost exclusively of Nikolai greenstones or andesitic breccias of the Slana Spur Formation from the Wrangellia terrane, amphibolites from the Gulkana River complex, and phyllites and mica quartzites from the Yukon–Tanana terrane. Nonetheless, these latter rock types could comprise a minor fraction of the middle crust.

Compressional-wave velocities in the upper crust of the Wrangellia terrane are higher than those in the Yukon–Tanana terrane (Fig. 6). Laboratory measurements (Fig. 10) suggest that the higher upper crustal velocities in the Wrangellia terrane may reflect the presence of moderate (up to 30%) amounts of higher velocity andesites, amphibolites, or greenstone units.

V_p/V_s ratios vary between 1.67 and 1.77 for laboratory samples best matching our model (Fig. 10). In Table 3 we assumed a V_p/V_s ratio within this range, 1.73, to convert measured compressional-wave to shear-wave velocities.

Table 7
Sample Lithologies (Ordered by Increasing Latitude)

Sample	Latitude	Longitude	Lithology	Formation	Terrane
TA-14	62.63361	145.460000	Amphibolite	Gulkana River Complex	Gulkana
TA-15	62.66028	145.475278	Amphibolite	Gulkana River Complex	Gulkana
TA-16	62.68361	145.445000	Metagranodiorite	Gulkana River Complex	Gulkana
TA-27	62.82222	145.488889	Quartz diorite	Gulkana River Complex	Gulkana
TA-17	62.83111	145.473333	Metaandesite	Gulkana River Complex	Gulkana
TA-18	62.97583	145.448611	Greenstone	Nikolai Greenstone	Wrangellia
TA-19	63.09000	145.618889	Greenstone	Nikolai Greenstone	Wrangellia
TA-22	63.31111	145.705556	Andesite breccia	Slana Spur	Wrangellia
TA-28	63.33611	145.694444	Metaandesite		Wrangellia
TA-21	63.43333	145.788889	Mica-Quartz Schist	Jarvis Creek	Yukon–Tanana
TA-20	63.46139	145.791667	Mica-Quartz Schist	Jarvis Creek	Yukon–Tanana
TA-29	63.57972	145.861111	Mica-Quartz Schist		Yukon–Tanana
TA-115	63.66389	145.841667	Mica-Quartz Schist	Jarvis Creek	Yukon–Tanana
TA-114	63.73611	145.877778	Mica-Quartz Schist	Jarvis Creek	Yukon–Tanana
TA-112	63.81111	145.783333	Tonalite gneiss	Donnelly Dome	Yukon–Tanana
TA-113	63.81111	145.783333	Tonalite gneiss	Donnelly Dome	Yukon–Tanana
TA-42	64.15833	145.858333	Augen Gneiss		Yukon–Tanana
TA-47	64.26111	146.130556	Gneiss		Yukon–Tanana
TA-45	64.34167	146.852778	Andesite		Yukon–Tanana
TA-46	64.34444	146.825000	Augen Gneiss		Yukon–Tanana
TA-44	64.50000	146.969444	Mica-Quartzite		Yukon–Tanana
TA-43	64.73889	147.066667	Slate-Phyllite		Yukon–Tanana
TA-56	65.08889	147.719444	Mica-Quartz Schist	Fairbanks Schist	Yukon–Tanana
TA-57	65.08889	147.719444	Mica Quartzite	Fairbanks Schist	Yukon–Tanana

Table 8
Compressional-Wave Velocity (km/sec) of Rocks of Kahiltna Formation as a Function of Confining Pressure

Press (MPa)	TA-194B	TA-194C	TA-194D	Mean
10	5.87	5.98	5.72	5.85
30	6.00	6.09	6.04	6.04
50	6.06	6.14	6.22	6.14
70	6.11	6.17	6.34	6.21
100	6.15	6.21	6.45	6.27
200	6.22	6.28	6.60	6.37
300	6.26	6.33	6.66	6.42
400	6.29	6.36	6.71	6.45
500	6.32	6.38	6.74	6.48
600	6.34	6.40	6.77	6.50
700	6.35	6.42	6.79	6.52
800	6.37	6.43	6.81	6.54
900	6.38	6.45	6.83	6.55
1000	6.39	6.46	6.84	6.56
Density, kg/m^3	2778	2765	2960	2834

N. I. Christensen (unpublished data, 2003).

Measurements for several samples (TA-20, TA-21, TA-43, and TA-57) yielded unusually low V_p/V_s and Poisson's ratios (Tables 5, 6), not thought typical of these rocks, and are not plotted on Figure 10.

At constant hydrostatic pressure, linear regression of mean compressional-wave velocity and density for 28 samples of the Wrangellia, Yukon–Tanana, and Kahiltna terranes (Tables 4–6, 8) define empirical relationships between these properties (Fig. 11). At 100 MPa, corresponding to a depth of about 3 km, this relationship is:

$$\rho(\text{kg/m}^3) = 348\ V_p(\text{km/sec}) + 646. \quad (1)$$

At 1000 MPa, corresponding to a depth of about 30 km, we find:

$$\rho(\text{kg/m}^3) = 418\ V_p(\text{km/sec}) + 75. \quad (2)$$

Both relationships fit the observations within a maximum error of 100 kg/m^3. The correlation coefficient is higher for a confining pressure of 1000 MPa ($R^2 = 0.92$) but remains compelling at 100 MPa ($R^2 = 0.90$). This linear relationship (Fig. 11) results in the close correspondence between the isostatic gravity and the tomography model (Fig. 8).

Moho Geometry

Our inference of a 45- to 50-km crustal thickness near the Denali fault (Fig. 12) agrees with other studies. TACT seismic lines south of the Denali fault zone (Goodwin *et al.*, 1989; Fuis *et al.*, 1991) demonstrate that a 45- to 50-km-thick crust occupies a region about 180 km wide (Fig. 12). Teleseismic receiver function analysis of broadband data reveals a 46- to 47-km-thick crust south of the main strand of the Denali fault along the Parks Highway (at 149°W) (Meyers *et al.*, 2001; Meyers-Smith *et al.*, 2002).

Our inference of a thin, 28-km-thick crust in the Yukon–

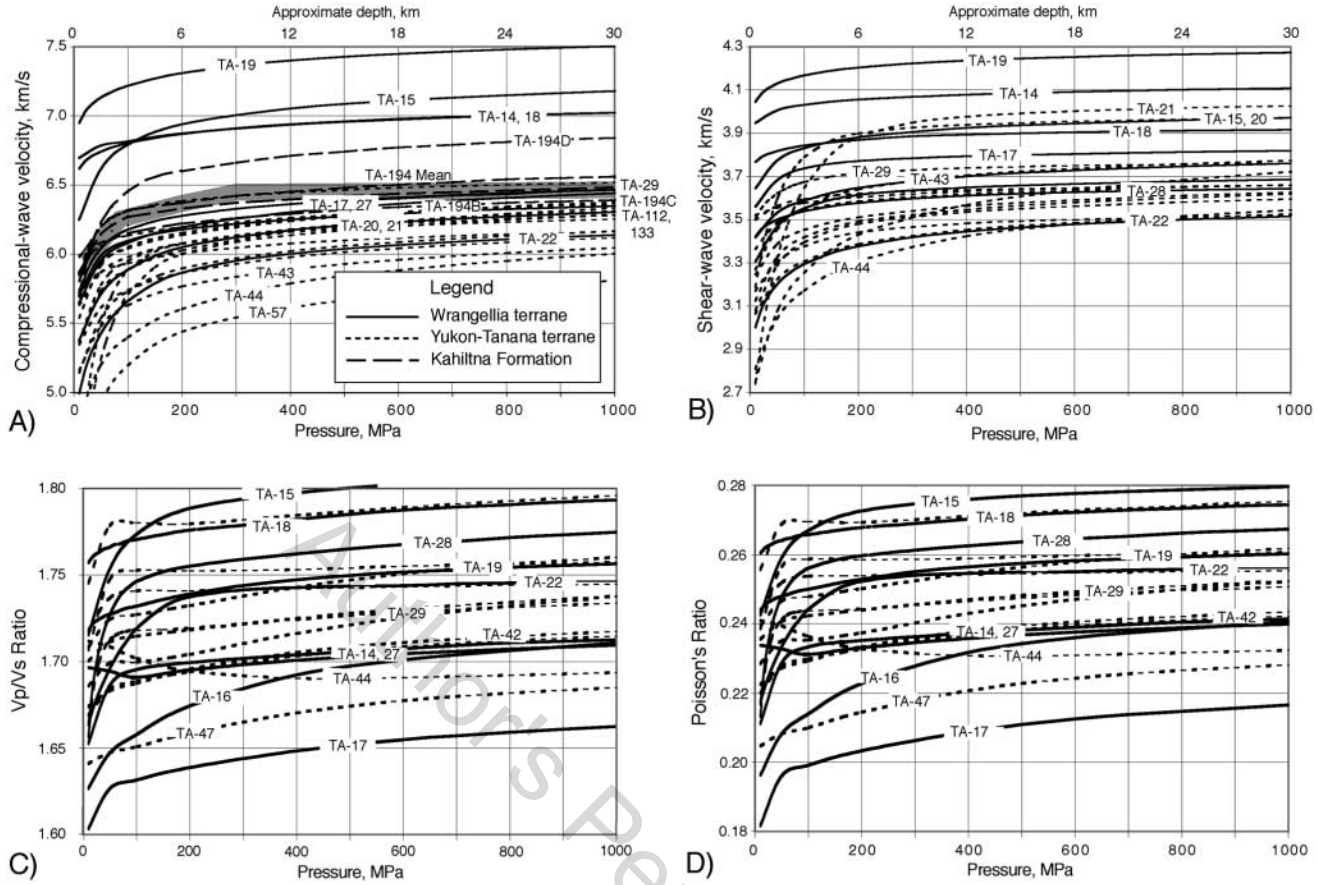

Figure 10. Comparison of laboratory measurements of (A) compressional- and (B) shear-wave velocities for samples of the Gulkana, Wrangellia, and Yukon–Tanana terranes, and for the Kahiltna Formation (Tables 4–6, 8). Thick gray shaded line in (A) shows range of compressional-wave velocities determined from the TACT 1987 line. (C) V_p/V_s and (D) Poisson's ratios for these samples.

Tanana terrane from *Pn* travel times also agrees with other studies. Thin (28–32 km), low-velocity crust (6.1–6.4 km/sec) beneath the Yukon–Tanana terrane (Fig. 12) was documented by Beaudoin *et al.* (1992) from refraction studies centered at Delta Junction and by Searcy *et al.* (1996) from teleseismic receiver function analysis near Fairbanks. Lowe and Cassidy (1995) also reported thin crust north of the Denali fault in the Yukon Territory of Canada, where the crustal thickness was measured as 35 and 39 km at Dawson and Whitehorse, respectively. Based on field mapping, structural fabric analysis, and isotopic data, Pavlis *et al.* (1993) argued that the Yukon–Tanana terrane underwent amagmatic extension during the mid-Cretaceous, which would explain the thin crust there.

The geometry of the transition between the thick crust in the Alaska Range and the thin crust beneath the Yukon–Tanana terrane is not imaged by our analysis. We show it as being transitional in Figure 12, but it could be more step-like. In any case, our model provides no evidence for a steep step in the Moho across the Denali fault zone (Fig. 12).

A number of different origins for the large crustal thickness beneath the Alaska Range are proposed. Fuis and Plafker (1991) suggested three different means of forming the thick crust beneath the Peninsular and Wrangellia terranes, including (1) Cretaceous overthrusting of North America by the Peninsular-Wrangellia terrane, (2) late Cretaceous-early Tertiary tectonic underplating of the Peninsular-Wrangellia terrane by accretionary rocks and oceanic crust during the rapid subduction of the Kula plate, and (3) Cretaceous or possibly Tertiary magmatic underplating of the crust of the Peninsular-Wrangellia terrane by a cryptic arc. Plafker *et al.* (1989) proposed a fourth alternative: underthrusting of the Kluane arc beneath the Alaska Range during the collision of the Wrangellia and Yukon–Tanana terranes.

In any case, one-dimensional forward modeling indicates that the 50-km thick crust beneath the Denali fault produces large amplitude *PmP* wide-angle reflections from surface sources at ranges between 130 and 350 km. Enhancement of strong ground motions by *SmS* wide-angle reflections from surface sources is expected only in this distance range, which includes the distances to Fairbanks and Anchorage. In qualitative terms, the general southward dip

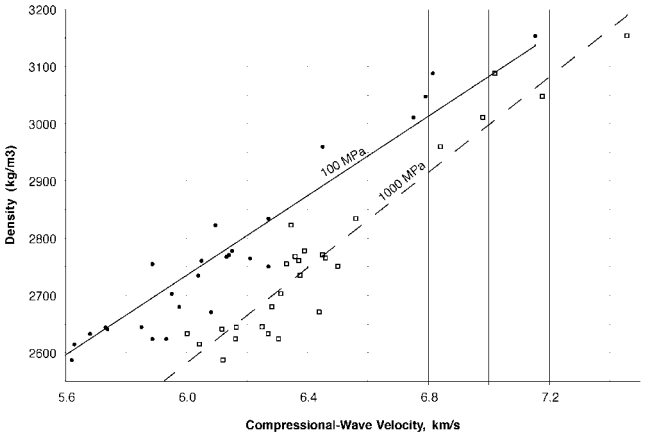

Figure 11. Compressional-wave velocity versus density at hydrostatic confining pressures of 100 and 1000 MPa. Values, except for Kahiltna Formation given in Table 8, are means. Filled circles and squares show measurements at a hydrostatic confining pressure of 100 MPa and 1000 MPa, respectively. Solid and dashed lines show linear regressions to measurements at a hydrostatic confining pressure of 100 MPa and 1000 MPa, respectively.

of the Moho (Fig. 12) would defocus *SmS* arrivals from the Denali fault traveling toward Anchorage and would focus *SmS* arrivals from the Denali fault traveling toward Fairbanks. Although a detailed test of this hypothesis lies outside the scope of the present study, we note that in agreement with this prediction, peak accelerations observed in Anchorage are nearly 5 times smaller than those in Fairbanks (Frankel, 2005), even though Anchorage is only 1.25 and 1.66 times as far from the three earthquake subevents as Fairbanks. Perhaps crustal defocusing, in addition to directivity and source complexity effects, accounts for some of this apparent discrepancy.

Summary

We report crustal-scale compressional- and shear-wave velocity models for the Denali fault from TACT seismic data acquired in 1986 and 1987. We interpret a low velocity zone in the upper crust along the Denali fault zone as a broad zone of fault damage associated with the Denali fault zone and nearby thrust faults. This broad low-velocity zone is associated with an isostatic gravity low that closely corresponds with the geometry of the 6 km/sec isocontour. Our seismic model, gravity data, and magnetotelluric data image the Denali fault zone as a near vertical structure to a depth of at least 30 km (Fisher *et al.*, 2004). Weak wide-angle reflections are consistent with the absence of significant velocity contrasts across the Denali fault zone below 10 km depth. The average compressional-wave velocity of the crust is low relative to normal continental crust, below 6.5 km/sec, consistent with laboratory measurements of rock samples from along our transect. The inferred 50-km crustal thickness beneath the Denali fault zone is transitional between thicker crust beneath the Wrangellia terrane to the south and extended Yukon–Tanana terrane crust to the north: our model provides no evidence for an abrupt step in Moho thickness across the fault zone.

The TACT seismic reflection and refraction lines, as well as Denali fault earthquake aftershocks, provide evidence for thrust faulting within a flower structure (e.g., Harding, 1985), including the McCallum-Slate Creek and Donnelly Dome-Granite Mountain thrust faults, located on opposite sides of the Denali fault zone. Aftershocks of the Denali fault earthquake in the vicinity of our seismic lines appear to de-

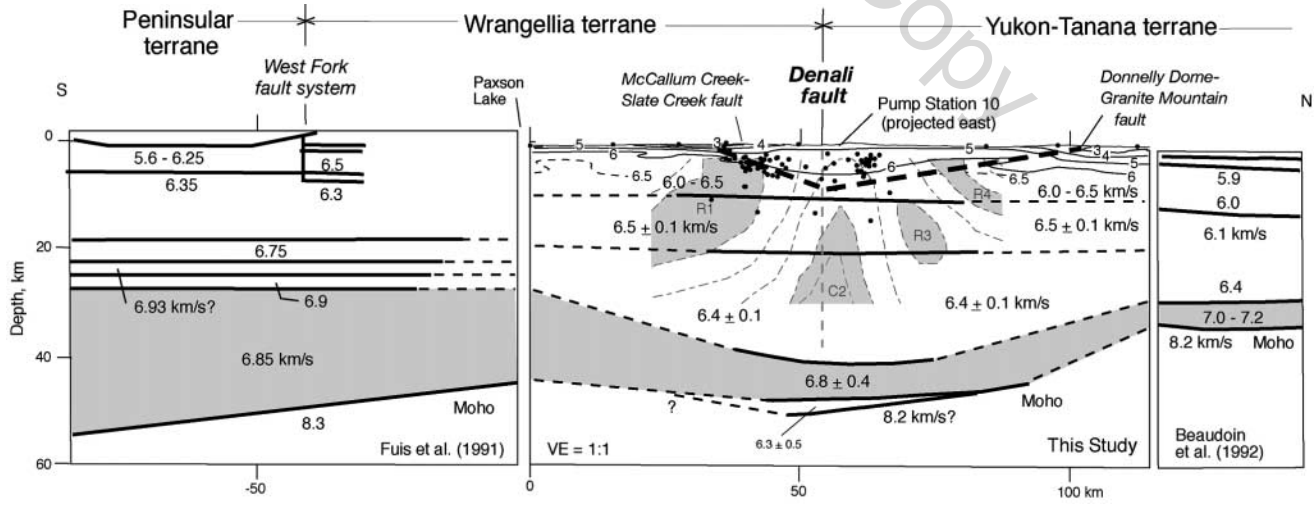

Figure 12. Compilation of compressional-wave velocity models near the Denali fault. Our model is shown in the middle panel. Models by Fuis *et al.* (1991) and Beaudoin *et al.* (1992) illustrate northward thinning of the crust beneath the Denali fault. Format as for Figure 7.

fine a shallow, low-angle, south-dipping fault that is truncated at depth by the nearly vertical Denali fault zone.

Data Sources

SEG-Y formatted versions of the TACT 1987 common receiver gathers are available on a single 92-Mbyte 8-mm tape from the IRIS Data Management Center (www.iris.edu/about/PASSCAL/regions/AK.htm#2000-035).

Acknowledgments

The USGS's Deep Continental Studies and Earthquake Programs supported this work.

For their assistance in collecting the TACT 1987 seismic refraction data, we thank E. Ambos, B. Beaudoin, P. Berge, J. Cotton, E. Criley, E. Greene, R. Kaderabek, W. Kohler, J. Luetgert, R. Luzitano, R. McClearn, W. Mooney, J. Murphy, B. Page, R. Page, D. Reneau, J. Shimata, J. Van Schaack, D. Whitman, and J. Wilson. We are indebted to the U.S. Bureau of Land Management, the State of Alaska, Ahtna, Inc., and the Alyeska Pipeline Service Company for permission to conduct our refraction profiling on land under their jurisdictions. R. Luzitano picked first-arrival travel times used for the TACT 1987 line. R. Andrus, M. Bennett, K. Fogleman, T. Holzer, and W. Savage helped locate and interpret borehole data from Pump Station 10. Digital coordinates for the TACT 1986 line were picked using the TopoZone.com website. Shirley Baher, Bruce Beaudoin, John Cassidy, Donna Eberhart-Phillips, Mike Fisher, Peter Haeussler, Kate Miller, and Paul Spudich reviewed earlier versions of this report. Rick Blakely generated maps showing simple Bouguer, complete Bouguer, and isostatic gravity for the study area, and he plotted the profile used in Figure 9A.

References

Aleinikoff, J. N., and W. J. Nokleberg (1985). Age of Devonian igneous-arc terranes in the northern Mount Hayes quadrangle, eastern Alaska Range, *U.S. Geol. Surv. Circ. 967*, 44–49.

Beaudoin, B. C., G. S. Fuis, W. D. Mooney, W. J. Nokleberg, and N. I. Christensen (1992). Thin, low-velocity crust beneath the southern Yukon–Tanana terrane, east-central Alaska: results from Trans-Alaska Crustal Transect refraction/wide-angle reflection data, *J. Geophys. Res.* **97,** 1921–1942.

Beaudoin, B. C., G. Perkins, G. S. Fuis, and J. H. Luetgert (1989). Data report for the 1987 seismic refraction survey: Alaska Range and Fairbanks South deployments, *U.S. Geol. Surv. Open-File Rept. 89-321*, 114 pp.

Brocher, T. M. (2003). Detonation charge size versus coda magnitude relations in California and Nevada, *Bull. Seism. Soc. Am.* **93,** 2089–2105.

Brocher, T. M., W. J. Nokleberg, N. I. Christensen, W. J. Lutter, E. L. Geist, and M. A. Fisher (1991). Seismic reflection/refraction mapping of faulting and regional dips in the eastern Alaska Range, *J. Geophys. Res.* **96,** 10,233–10,249.

Chester, F. M., D. L. Kirschner, and J. S. Chester (1999). Extreme localization of slip during earthquake rupture; field evidence from the Punchbowl and San Gabriel faults, San Andreas system, California, *EOS*. **80,** no. 46 (suppl., abstract), p. 689.

Christensen, N. I. (1979). Compressional wave velocities in rocks at high temperatures and pressures, critical thermal gradients, and crustal low-velocity zones, *J. Geophys. Res.* **84,** 6849–6857.

Christensen, N. I., and W. D. Mooney (1995). Seismic velocity structure and composition of the continental crust: a global view, *J. Geophys. Res.* **100,** 9761–9788.

Eberhart-Phillips, D., P. J. Haeussler, J. T. Freymueller, A. D. Frankel, C. M. Rubin, P. Craw, N. A. Ratchkovski, G. Anderson, A. J. Crone, T. E. Dawson, H. Fletcher, R. Hansen, E. L. Harp, R. A. Harris, D. P. Hill, S. Hreinsdottir, R. W. Jibson, L. M. Jones, D. K. Keefer, C. F. Larsen, S. C. Moran, S. F. Personius, G. Plafker, B. Sherrod, K. Sieh, and W. K. Wallace (2003). The 2002 Denali fault earthquake, Alaska: a large magnitude, slip-partitioned event, *Science* **300,** 1113–1118.

Ellsworth, W. L., M. Celebi, J. R. Evans, E. G. Jensen, R. Kayen, M. C. Metz, D. J. Nyman, J. W. Roddick, P. Spudich, and C. D. Stephens (2004). Near-field ground motion of the *M* 7.9 November 3, 2002 Denali fault, Alaska, earthquake recorded at Pump Station 10, *Earthquake Spectra* **20,** 597–616.

Fisher, M. A., W. J. Nokleberg, N. A. Ratchkovski, L. Pellerin, J. M. Glen, T. M. Brocher, and J. Booker (2004). Geophysical investigation of the Denali fault and Alaska Range orogen within the aftershock zone of the October-November 2002, $M = 7.9$ Denali fault earthquake, *Geology* **32,** 269–272.

Fletcher, H. J. (2002). Tectonics in interior Alaska from GPS measurements, *Ph.D. Thesis*, University of Alaska, Fairbanks, 257 pp.

Foster, H. L., T. E. C. Keith, and W. D. Menzie (1987). Geology of east-central Alaska, *U.S. Geol. Surv. Open-File Rept. 87-188*, 59 pp.

Frankel, A. (2005). Rupture process of the *M* 7.9 Denali fault, Alaska, earthquake: subevents, directivity, and scaling of high-frequency ground motions, *Bull. Seism. Soc. Am.* **94,** no. 6B, S234–S255.

Fuis, G. S., and G. Plafker (1991). Evolution of deep structure along the Trans-Alaska Crustal Transect, Chugach Mountains and Copper River Basin, southern Alaska, *J. Geophys. Res.* **96,** 4229–4253.

Fuis, G. S., E. L. Ambos, W. D. Mooney, N. I. Christensen, and E. Geist (1991). Crustal structure of accreted terranes in southern Alaska, Chugach Mountains and Copper River Basin, from seismic refraction results, *J. Geophys. Res.* **96,** 4187–4227.

Goodwin, E. B., G. S. Fuis, W. J. Nokleberg, and E. L. Ambos (1989). The crustal structure of the Wrangellia terrane along the East Glenn Highway, eastern-southern Alaska, *J. Geophys. Res.* **94,** 16,037–16,057.

Haeussler, P. J., D. P. Schwartz, T. E. Dawson, H. D. Stenner, J. J. Lienkaemper, B. Sherrod, F. R. Cinti, P. Montone, P. Crow, A. J. Crone, and S. F. Personius (2005). Surface rupture and slip distribution of the Denali and Totschunda faults in the 3 November 2002 **M** 7.9 Earthquake, Alaska, *Bull. Seism. Soc. Am.* **94,** no. 6B, S23–S52.

Harding, T. P. (1985). Seismic characteristics and identification of negative flower structures, positive flower structures, and positive structural inversion, *AAPG Bull.* **69,** 582–600.

Hreinsdottir, S., J. T Freymueller, and R. Burgmann (2003). Coseismic slip distribution of the Denali fault earthquake as estimated from GPS measurements, *EOS*, **84,** (Fall Meet. Suppl.), abstract S11H-07.

Hudson, T., and F. R. Weber (1977). The Donnelly Dome and Granite Mountain faults, south-central Alaska, *U.S. Geol. Surv. Circ. C 751-B*, B64–B66.

Jones, D. L., N. J. Silberling, P. J. Coney, and G. Plafker (1987). Lithotectonic terrane map of Alaska (west of the 141st meridian), 1 sheet, *U.S. Geol. Surv. Map MF-1874-A*, scale 1:2,500,000.

Kayen, R., E. Thompson, D. Minasian, B. Collins, E. R. S. Moss, N. Sitar, and G. Carver (2004). Geotechnical reconnaissance of the 2002 Denali fault earthquake, *Earthquake Spectra* **20,** 639–668.

Kohler, W. M., and G. S. Fuis (1992). Empirical dependence of seismic ground velocity on the weight of explosives, shotpoint site conditions, and recording distance for seismic-refraction data, *Bull. Seism. Soc. Am.* **82,** 2032–2044.

Li, Y. G., K. Aki, D. Adams, A. Hasemi, and W. H. K. Lee (1994). Seismic guided waves trapped in the fault zone of the Landers, California, earthquake of 1992, *J. Geophys. Res.* **99,** 11,705–11,722.

Li, Y. G., K. Aki, B. H. Chin, D. Adams, P. Beltas, and J. B. Chen (1995). Excitation and observation of fault-zone guided waves at the Landers fault zone, California, *Seism. Res. Lett.* **66,** 39.

Li, Y. G., W. L. Ellsworth, C. H. Thurber, P. E. Malin, and K. Aki (1997). Fault-zone guided waves from explosions in the San Andreas fault at Parkfield and Cienaga Valley, California, *Bull. Seism. Soc. Am.* **87,** 210–221.

Li, Y. G., P. C. Leary, K. Aki, and P. E. Malin (1990). Seismic trapped modes in the Oroville and San Andreas fault zones, *Science* **249,** 763–766.

Lowe, C., and J. F. Cassidy (1995). Geophysical evidence for crustal thickness variations between the Denali and Tintina fault systems in west-central Yukon, *Tectonics* **14,** 907–917.

Lutter, W. J., and R. L. Nowack (1990). Inversion for crustal structure using reflections from the PASSCAL Ouachita experiment, *J. Geophys. Res.* **95,** 4633–4646.

Lutter, W. J., R. L. Nowack, and L. W. Braile (1990). Seismic imaging of upper crustal structure using travel times from the PASSCAL Ouachita Experiment, *J. Geophys. Res.* **95,** 4621–4631.

Meyers, E. V., D. H. Christensen, A. Ferris, G. A. Abers, and A. Lucier (2001). Crustal thickness across the Alaska Range, *EOS* (Fall Meeting Suppl.) **82,** no. 47, abstract. T41C–0907.

Meyers-Smith, E. V., D. H. Christensen, and G. A. Abers (2002). Moho topography beneath the Alaska Range: results from BEARR, *EOS* (Fall Meeting Suppl.) **83,** no. 47, abstract. S52A–1073.

Mooney, W. D., and A. Ginzburg (1986). Seismic measurements of the internal properties of fault zones, *Pageoph* **124,** 141–157.

Morin, R. L., and J. M. G. Glen (2003). Principal facts for 408 gravity stations in the vicinity of the Talkeetna Mountains, south-central Alaska, *U.S. Geol. Surv. Open-File Rept. 03-27*, 15 pp.

Nokleberg, W. J., and J. N. Aleinikoff (1985). Summary of stratigraphy, structure, and metamorphism of Devonian igneous-arc terranes, northeastern Mount Hayes quadrangle, eastern Alaska Range, *U.S. Geol. Surv. Circ. 967*, 66–71.

Nokleberg, W. J., N. R. D. Albert, G. C. Bond, P. L. Herzon, R. T. Miyaoka, W. H. Nelson, D. H. Richter, T. E. Smith, J. H. Stout, W. Yeend, and R. E. Zehner (1982). Geologic map of the southern part of the Mount Hayes quadrangle, Alaska, 1 sheet, *U.S. Geol. Surv. Open-File Rept. 82-52*, 26 pp, scale 1:250,000.

Nokleberg, W. J., J. N. Aleinikoff, and I. M. Lange (1986). Cretaceous deformation and metamorphism in the northeastern Mount Hayes quadrangle, eastern Alaska Range, *U.S. Geol. Surv. Circ. 978*, 64–69.

Nokleberg, W. J., J. N. Aleinikoff, I. M. Lange, S. R. Silva, R. T. Miyaoka, C. E. Schwab, and R. E. Zehner (1992a). Map, tables, and summary of fossil and isotopic age data, Mount Hayes quadrangle, eastern Alaska Range, Alaska, *U.S. Geol. Surv. Misc. Field Studies Map 1996-D* (scale 1:250,000).

Nokleberg, W. J., J. N. Aleinikoff, I. M. Lange, S. R. Silva, R. T. Miyaoka, C. E. Schwab, and R. E. Zehner (1992b). Preliminary geologic map of the Mount Hayes quadrangle, eastern Alaska Range, Alaska, *U.S. Geol. Surv. Open-File Rept. 92-594*, scale 1:250,000.

Nokleberg, W. J., H. L. Foster, and J. N. Aleinikoff (1989). Geology of the northern Copper River basin, eastern Alaska Range, and southern Yukon–Tanana Basin, southern and east-central Alaska, *in Sedimentation and Tectonics of Western North America, Alaskan Geological and Geophysical Transect, Field Trip Guidebook T104*, W. J. Nokleberg and M. A. Fisher (Editors), Vol. **5,** American Geophysical Union, Washington, D.C., 34–63.

Nokleberg, W. J., D. L. Jones, and N. J. Siberling (1985). Origin and tectonic evolution of the Maclaren and Wrangellia terranes, eastern Alaska Range, Alaska, *Geol. Soc. Am. Bull.* **96,** 1251–1270.

Nowack, R. L., and W. J. Lutter (1988). A note on the calculation of covariance and resolution, *Geophys. J.* **95,** 205–207.

Pavlis, T. L., V. B. Sisson, H. L. Foster, W. J. Nokleberg, and G. Plafker (1993). Mid-Cretaceous extensional tectonics of the Yukon–Tanana terrane, Trans-Alaska Crustal Transect (TACT), east-central Alaska, *Tectonics* **12,** 103–122.

Plafker, G., C. D. Blome, and N. J. Silberling (1989). Reinterpretation of lower Mesozoic rocks on the Cilkat Peninsula, Alaska, as a displaced fragment of Wrangellia, *Geology* **17,** 3–6.

Plafker, G., T. Hudson, and D. H. Richter (1977). Preliminary observations of late Cenozoic displacements along the Totschunda and Denali fault systems, *U.S. Geol. Surv. Circ. 751B*, B67–B69.

Ratchkovski, N. A., A. Hansen, J. C. Stachnik, T. Cox, O. Fox, L. Rao, E. Clark, M. Lafevers, S. Estes, J. B. MacCormack, and T. Williams (2003). Aftershock sequence of the M_w 7.9 Denali, Alaska, earthquake of 3 November 2002 from the regional seismic network data, *Seism. Res. Lett.* **76,** 742–751.

Ridgway, K. D., J. M. Trop, W. J. Nokleberg, C. M. Davidson, and K. R. Eastham (2002). Mesozoic and Cenozoic tectonics of the eastern and central Alaska Range: progressive basin development and deformation in a suture zone, *Geol. Soc. Am. Bull.* **114,** 1480–1504.

Ridgway, K. D., J. M. Trop, and A. R. Sweet (1997). Thrust-top basin formation along a suture zone, Cantwell basin, Alaska Range: implications for development of the Denali fault system, *Geol. Soc. Am. Bull.* **109,** 505–523.

Rose, A. W. (1967). Geology of the upper Chistochina river area, Mt. Hayes quadrangle, Alaska, *Alaska Div. Geol. Geophys. Surv. Geol. Rept. 28*, 39 pp., 2 plates.

Searcy, C. K., D. H. Christensen, and G. Zandt (1996). Velocity structure beneath College Station, Alaska (COL), from inversion of receiver functions, *Bull. Seism. Soc. Am.* **86,** 232–241.

Sheriff, R. E., and L. P. Geldart (1995). *Exploration Seismology*, Cambridge University Press, Cambridge, U.K., 592 pp.

Spudich, P., and K. B. Olsen (2001). Fault zone amplified waves as a possible seismic hazard along the Calaveras fault in central California, *Geophys. Res. Lett.* **28,** 2533–2536.

Stanley, W. D., V. F. Labson, W. J. Nokleberg, B. Csejtey, Jr., and M. A. Fisher (1990). The Denali fault system and Alaska Range of Alaska: evidence for underplated Mesozoic flysch from magnetotelluric surveys, *Geol. Soc. Am. Bull.* **102,** 160–173.

Stone, D. B., R. A. Page, and J. N. Davies (1986). Trans-Alaska lithosphere investigation: program prospectus, *U.S. Geol. Surv. Circ. C0984*, 24 pp.

Stout, J. H., and C. G. Chase (1980). Plate kinematics of the Denali fault system, *Can. J. Earth Sci.* **17,** 1527–1537.

Stout, J. H., J. B. Brady, F. Weber, and R. A. Page (1973). Evidence for Quaternary movement on the McKinley strand of the Denali fault in the Delta River area, Alaska, *Geol. Soc. Am. Bull.* **84,** 939–947.

U.S. Geological Survey
345 Middlefield Rd.
MS 977
Menlo Park, California 94025
(T.M.B., G.S.F.)

Dept. of Geology and Geophysics
1215 W. Dayton St.
University of Wisconsin
Madison, Wisconsin 53706
(W.J.L., N.I.C.)

Alaska Earthquake Information Center
Geophysical Institute, University of Alaska
Fairbanks, Alaska 99775
(N.A.R.)

Manuscript received 4 February 2004.